Supplementary Material for:

SDS22 selectively recognizes and traps metal-deficient, inactive PP1

Meng S. Choy[1,#], Thomas M. Moon[1,#], Rini Ravindran[2,#], Johnny A. Bray[1], Lucy C. Robinson[2], Tara L. Archuleta[1], Wuxian Shi[3], Wolfgang Peti[1], Kelly Tatchell[2,*] & Rebecca Page[1,*]

Table of Contents

1. **Methods**
2. **Table S1:** *Data collection and refinement statistics*
3. **Table S2**: *SPR binding kinetics for the association of NIPP1 with PP1 variants*
4. **Table S3**: *T_ms and Michalis-Menten activity constants of PP1 variants*
5. **Table S4:** *Yeast strains used in this study*
6. **Table S5:** *Key resources*
7. **Figure S1**. *Sequence alignment of the PPP family and SDS22 structure*.
8. **Figure S2**. *PP1 active site metals differ in otherwise identical SDS22:PP1 reconstituted versus coexpressed complexes*.
9. **Figure S3**. *SPR sensorgrams for SDS22 and PP1 variants.*
10. **Figure S4**. *Time-course of M1 metal loss in PP1 and SDS22 binding to M1-metal free PP1*.
11. **Figure S5**. *SPR sensorgrams for NIPP1 and PP1 variants.*
12. **Figure S6:** *Mn^{2+} is unable to dissociate assembled SDS22:PP1 complexes*
13. **Figure S7.** *Crystal structure of the H66K*.
14. **Figure S8**. *Mn^{2+} competes with SDS22 for PP1 binding and the structures of PP1 variants Y134K and Y134A*
15. **Figure S9**. *A platform for monitoring protein binding to nascent PP1*.
16. **Figure S10**. *Low levels of Sds22 are recruited to the bud neck in cells expressing the Y133A and K146A K149A Glc7 variants.*
17. **Figure S11**. *Mutations altering the GLC7 active site disrupt normal localization due to SDS22 sequestration*.

www.pnas.org/cgi/doi/10.1073/pnas.1908718116

METHODS

Plasmid construction. SDS22$_{56–360}$, PP1α$_{1-300}$, I2$_{9-165}$, I3$_{1-126}$, and Spinophilin$_{417-602}$ genes were cloned into a modified pcDNA3.4 vector (pcDNA3.4_K_RP1B). The pcDNA3.4_K_RP1B vector contains a Kozak consensus sequence, an N-terminal His$_6$-tag, a TEV cleavage site and a multiple cloning site (the latter elements are derived from the *E. coli* RP1B expression vector;) following the pcDNA3.4 human cytomegalovirus (CMV) promoter. This plasmid was amplified and purified using the PureLink HiPure Plasmid Maxiprep Kit (ThermoFisher). PP1 variants D64A, H66K, Y134F, Y134K, Y134A and G135A were generated using QuikChange mutagenesis (Agilent) following the manufacturer's protocol.

Protein expression. SDS22$_{56-360}$ and PP1α$_{1-300}$ were expressed in Expi293F cells (ThermoFisher) at a ratio of 1.0 µg DNA per mL of final transfection culture volume. The SDS22$_{56-360}$:PP1α$_{1-300}$ complex was coexpressed in Expi293F cells at a 1:1 ratio of 1.0 µg total DNA per milliliter of final transfection culture volume. Transfections were performed using 600 ml medium (Gibco Expi293 Expression Medium) in 2 L baffled flasks according to the manufacturer's protocol in a humidified incubator at 37°C and 6.5% CO_2 under shaking (125 rpm). On the day of transfection, the cell density was between 3-5 × 10^6 cells ml^{-1}. Prior to transfection, the Expi293F cells were seeded at 2.9 × 10^6 cells ml^{-1} in 85% of the final transfection volume. SDS22$_{56-360}$:PP1α$_{1-300}$ DNA (1:1 ratio) was mixed with Opti-MEM Reduced Serum Medium (ThermoFisher); in a separate tube, Expifectamine reagent (ThermoFisher) was mixed with Opti-MEM medium. These mixtures were incubated separately for 5 min, then the DNA and Expifectamine mixtures were combined and incubated for an additional 20 min. The final transfection mixture was then added to the cells. Enhancer 1 and Enhancer 2 were added to the cells 18–20 h post-transfection. After an additional 24–28 h, the cells were harvested and the pellet was stored at −80°C.

I2$_{9-165}$:PP1α$_{1-300}$, I3$_{1-126}$:PP1α$_{1-300}$ and Spinophilin$_{417-602}$:PP1α$_{1-300}$ complexes were expressed in Expi293F cells (ThermoFisher) at a 1:1 ratio of 0.8 µg total DNA per milliliter of final transfection-culture volume. Transfections were performed using 60 ml in 250 mL baffled flasks (Corning) using the same conditions as for SDS22$_{56-360}$:PP1α$_{1-300}$. Alternatively, FectoPro (Polyplus) was used for transfection. Here, the DNA mixture was added to FectoPro, mixed, and incubated for 10 min. This final transfection mixture was added to the cells. Boost reagent (Polyplus) and 2 mM (final concentration) Valproic acid were added to the cells 4 h post-transfection. Cells were harvested 48 h post transfection and the pellets stored at −80°C. Wt-PP1 and variants were expressed according to established protocols (1). SDS22$_{56-360}$ was expressed as previously described (2). NIPP1$_{158-216}$ was expressed as previously described (3).

Protein purification. WT PP1 and PP1 variants were purified as previously described (1). SDS22$_{56-360}$ was purified as previously described (2). NIPP1$_{158-216}$ was purified as previously described (3). The SDS22$_{56-360}$:PP1α$_{1-300}$ complex coexpressed in Expi293F cells (coexpressed SDS22:PP1) was purified as follows. Expi293F cells coexpressing SDS22$_{56-360}$:PP1α$_{1-300}$ were

lysed in His_6-tag Lysis Buffer (25 mM Tris pH 8.0, 500 mM NaCl, 5 mM imidazole, 0.1% Triton X-100, EDTA-free protease inhibitor tablet [Roche]) using high-pressure homogenization (Avestin C3). The resulting lysate was centrifuged at 40,000 *x*g for 45 min and the clarified supernatant was filtered through 0.22 µm polyethersulfone (PES) membrane filter (Millipore) before loading onto a HisTrap HP column (GE Healthcare). The column was washed with 50 mL of His-tag Buffer A (25 mM Tris pH 8.0, 500 mM NaCl, 5 mM imidazole), followed by 6% His-tag Buffer B (25 mM Tris pH 8.0, 500 mM NaCl, 250 mM imidazole) until the 280 nm UV trace reached baseline. Column-bound proteins were washed with 40 mL of 5 mM ATP-Mg^{2+} in His-tag buffer A at a flow rate of 0.5 mL/min to remove contaminants. The coexpressed SDS22:PP1 complex was eluted with a gradient elution of 6-65% His-tag buffer B at a flow rate of 2 mL/min. The peak fractions were pooled and dialyzed overnight in Dialysis Buffer (20 mM Tris pH 8.0, 250 mM NaCl, 0.5 mM TCEP) in the presence of TEV to cleave the His_6-tag. Subtraction purification was performed to remove the His_6-tag and TEV and the flow-through that contain the coexpressed SDS22:PP1 complex was purified using size exclusion chromatography (SEC, Superdex 75 26/60, GE Healthcare) in SDS22:PP1 complex SEC buffer (20 mM Tris pH 8.0, 250 mM NaCl, 0.5 mM TCEP). The fractions containing the SDS22:PP1 complex were pooled and concentrated to 6.5 mg/mL for crystallization.

The reconstituted $SDS22_{56\text{-}360}$:$PP1\alpha_{1\text{-}300}$ complex (reconstituted SDS22:PP1) was purified as follows. Bacteria expressing His_6-PP1 were lysed in PP1 Lysis Buffer (25 mM Tris pH 8.0, 700 mM NaCl, 5 mM imidazole, 1 mM $MnCl_2$, 0.1% Triton X-100, EDTA-free protease inhibitor tablets [Roche]) using high-pressure homogenization (Avestin C3). The lysate was clarified by centrifugation at 40,000 *x*g for 45 min and filtered through 0.22 µm PES membrane filter (Millipore) before loading onto Ni-NTA resin (Genesee Scientific). Bound His_6-PP1 was washed with PP1 buffer A (25 mM Tris pH 8.0, 700 mM NaCl, 5 mM imidazole, 1 mM $MnCl_2$) followed by 6% PP1 Buffer B (25 mM Tris pH 8.0, 700 mM NaCl, 250 mM imidazole, 1 mM $MnCl_2$). His_6-PP1 was eluted with 100% PP1 Buffer B and immediately subjected to size exclusion chromatography (SEC, Superdex 75 26/60, GE Healthcare) in SEC Buffer (20 mM Tris pH 8.0, 500 mM NaCl, 0.5 mM TCEP). Purified SDS22 was then incubated with His_6-PP1 at 1:1.2 (SDS22:PP1) molar ratio and dialyzed in complex SEC buffer (20 mM Tris pH 8.0, 250 mM NaCl, 0.5 mM TCEP) in the presence of TEV at 4°C to remove the His_6-tag from PP1. A second Ni-NTA purification was performed to remove the His_6-tag and TEV. The complex was again subjected to SEC in complex SEC buffer. The fractions containing the SDS22:PP1 complex were pooled and concentrated to 6.5 mg/mL for crystallization.

Crystallization and structure determination. Crystals of the coexpressed and reconstituted SDS22:PP1 complex were grown using hanging drop vapor diffusion at 16°C by mixing 3 µL of protein (7.5 mg/mL) with 1 µL of crystallization condition (14% w/v PEG 4000, 6% MPD, 0.1 M sodium/potassium phosphate pH 6.2). Drops were streak-seeded with micro-crystals obtained from the initial hits. Small, cylindrical, hollow crystals or large plates grew 3-5 days after seeding. Crystals were cryo-protected with crystallization condition supplemented with 35% MPD and

flash frozen in liquid nitrogen. X-ray diffraction data of the coexpressed SDS22:PP1 complex crystals (hollow cylindrical crystals) were collected at beamline 17-ID-2 (FMX) at NSLSII, Brookhaven National Laboratory, Long Island New York. A raster scan was used to identify the most strongly diffracting region on the crystal and the data collected using a helical/vector data collection protocol. X-ray diffraction data of the reconstituted $SDS22_{56-360}$:$PP1\alpha_{1-300}$ complex (large plates) were collected at the Stanford Synchrotron Radiation Lightsource (SSRL) beamline 12-2. The SDS22:PP1 datasets were phased using molecular replacement (Phaser as implemented in Phenix) using PP1 (PDBID 4MOV (1)) and SDS22 (PDBID 6HKW (4)) as search models. The space group of the coexpressed SDS22:PP1 is $P6_522$ and the space group of the reconstituted SDS22:PP1 is $P2_12_12$. Crystals of PP1 variants, Y134K, Y134K:microcystin-LR (MC), Y134A:MC and H66K:MC (Y134A, Y134K or H66K were incubated with MC at a 1:1 molar ratio on ice for 1 hr prior to crystallization) were obtained in 0.1 M MES, pH 6.0, 20 % PEG6000, 1 M LiCl at 16°C. All PP1 variant structures were solved by molecular replacement using PP1 (PDBID 4MOV) as the search model (space group of $P2_12_12_1$). All structures were completed using multiple cycles of building and refinement using Coot (5) and Phenix (6). Data collection and refinement statistics are reported in **Table S1**.

Surface Plasmon Resonance. SPR measurements were performed using a 4-channel Reichert 4SPR instrument fitted with autosampler and degassing pump (Reichert Technologies). SPR buffers containing 20 mM Tris pH 8.0, 500 mM NaCl, 0.5 mM TCEP, 0.05% Tween (with and without the addition of 1 mM $MnCl_2$ or 1 mM $ZnCl_2$) were prepared, sterile filtered, and degassed in autoclaved glassware prior to each experiment. Running buffer was used to prime and run both the sample and syringe pump reservoirs. Gold sensorchips modified with Ni-NTA-functionalized dextran (NiD50L; Xantec) were installed and equilibrated under flow conditions (100 µL/min) for ≥60 min at 25°C. Surface contaminants were cleared from the chip surface by a pair of 120 µL injections of 2 M NaCl and 10 mM NaOH during the equilibration step. Experiments were conducted at 25°C with a 5 Hz sampling rate and were initiated by injecting 120 µL of His_6-PP1 constructs (50 – 200 nM) diluted in 20 mM Tris pH 8.0, 500 mM NaCl, 1 mM $MnCl_2$, 0.5 mM TCEP, 0.05% Tween onto channels 1 and 2 for 120 s at 50 µL/min which resulted in between 150 – 350 µRIU of surface loading (channel 3 and 4 were used as reference surfaces). The sensorchip was allowed to equilibrate for 30 min at 50 µL/min prior to beginning the experiments. Purified $SDS22_{56-360}$ was diluted into running buffer from concentrated stocks and single 90 µL injections were applied for 90 s at 50 µL/min followed by a dissociation step of 180 s. Control experiments measuring $NIPP1_{158-216}$ binding to PP1 variants were set-up similarly except for a change in injection profile (60 µL injections of $NIPP1_{158-216}$ were applied for 60 s at 50 µL/min followed by a dissociation step of 120 s). For all experiments, two buffer blank injections were included to achieve double-referencing. Technical replicates were obtained by utilizing two channels per chip coupled with stripping of the sensorchip with 350 mM EDTA pH 8, reconditioning the surface with 10 mM NaOH to remove non-specifically bound PP1 aggregates, charging the surface with 40 mM $NiSO_4$, and reloading fresh PP1 onto the surface.

All replicates were generated with freshly diluted PP1 and SDS22. Single injection kinetic parameters were determined by curve-fitting using TraceDrawer software (Ridgeview Instruments AB) fit with a one-to-one model.

For kinetic titration experiments, PP1 and SDS22 were prepared as described above. A series of four buffer blank injections was followed by sequential injections of increasing concentrations of SDS22 without surface regeneration. For both blanks and SDS22, 90 µL of sample were injected for 90 s at 50 µL/min, followed by a 180 s dissociation step. Data was analysed by Scrubber (BioLogic Software) and ClampXP (Biosensor Data Analysis) using a kinetic titration model without mass transport (7). Time-dependence of metal dissociation was monitored by measuring the response of SDS22 binding normalized to the total amount of PP1 loaded on the surface. The wash step between PP1 loading and SDS22 injection was defined as 5, 14, 39, and 70 minutes to measure the changes in maximum SDS22 response relative to the amount of time PP1 was affixed to the chip. Single injection maximums were determined by curve-fitting using TraceDrawer software (Ridgeview Instruments AB) and fit with a one-phase exponential association model using Prism8 (GraphPad). Statistical analyses of SPR data were completed using SigmaPlot13 (Systat).

Protein stability measurements. Protein stability measurements (T_m) were performed on a Tycho NT.6 (Nanotemper) using standard capillaries using a 30°C/min ramp and evaluated using the Tycho NT.6 software version 1.2.0.750.

pNPP activity assay. All enzymatic assays were carried out in assay buffer (150 mM Bis-Tris pH 6.5, 150 mM NaCl) containing p-nitrophenyl phosphate (pNPP, 0 to 8000 µM) as substrate. PP1 (wt and variants) and PP1 complexes were diluted to a final concentration of 1 µM in PP1 buffer without $MnCl_2$ (20 mM Tris pH 8.0, 500 mM NaCl, 0.5 mM TCEP). The reaction was initiated by adding the substrate into the reaction buffer containing PP1 (final concentration of 0.1 µM; 96-well plate) and incubated at 30°C for 30 min. The reaction was stopped by adding 300 mM potassium phosphate, pH 10. The absorbance was measured at 405 nm using an Epoch2TC spectrophotometer (BioTek) and the data analyzed using GraphPad Prism8. Measured absorbance from blanks that contained substrate but no protein were subtracted from all measurements. The rate of dephosphorylation of pNPP was analyzed using the molar extinction coefficient for pNPP (18000 $M^{-1}cm^{-1}$) and an optical path length of 0.3 cm (96 well plates). All experiments were carried out in triplicate or more.

Pull-down experiments. To prepare lysates for pull-downs, 1 mL lysis buffer was added to each sample (lysis buffer: 50 mM Tris pH 8.5, 500 mM NaCl, 5 mM Imidazole, 0.1% Triton X-100, 1% NP40, 10 U/mL DNaseI, 1 mM $MnCl_2$, 5 mM $MgCl_2$, 1 protease inhibitor tablet [Roche/Millipore]). Cells in lysis buffer were then gently homogenized using a pipette. Cells were left on ice for 45 minutes to allow for full lysis (tubes were occasionally inverted). Lysed cells were centrifuged at 15,000 *x*g for 50 min. Pellets were washed with 1 mL lysis buffer and centrifuged at 15,000 *x*g

for 50 min. Lysis buffer was removed from pellets, and pellets were then prepped for gel sample (diluted loading dye into lysis buffer). The soluble fractions (supernatant at centrifugation step) were removed, added to 80 µL equilibrated Ni-NTA resin (equilibration buffer: 50 mM Tris pH 8.5, 500 mM NaCl, 5 mM Imidazole) and incubated 60 min. Samples were centrifuged at 1,500 *x*g for 8 min and the supernatant discarded. To wash the resin, 1 mL of equilibration buffer was added to each sample, the sample inverted and then centrifuged at 1,500 *x*g for 8 min. The resin washing steps were repeating a total of 3x. Bound protein(s) were eluted from the resin by adding 80 µL elution buffer (50 mM Tris pH 8.5, 500 mM NaCl, 500 mM Imidazole). After 10 min, the samples were centrifuged at 2,500 *x*g for 8 min. The eluate was then carefully removed and incubated with SDS-PAGE loading buffer. The pellet and eluate samples were then compared using SDS-PAGE (4-12%; Bio-Rad).

Western Blotting. Samples prepared from pulldowns were also examined by Western blot (n=4). Samples were loaded at equal volumes for SDS-PAGE (4–12%; Bio-Rad; Tris/Glycine/SDS Running Buffer; Precision Plus Protein Dual Color Standard was used to estimate the molecular weights). Proteins were transferred to a PVDF membrane by wet transfer and membranes were blocked in Li-COR Odyssey Blocking Buffer in PBS. Primary antibody, PP1γ (Sigma-PA5-21671), (diluted in Li-COR Odyssey Blocking Buffer) was added and incubated overnight at 4°C. Blots were washed in PBS-T, followed by incubation with the secondary antibody, Rabbit IgG StarBright Blue 520 (Bio-Rad 12005870, also in Li-COR Odyssey Blocking Buffer) for 60 min at room temperature. At this point, blots were washed in PBS-T and finally PBS. The PVDF membrane was dried before imaging. Fluorescent detection of the secondary antibody was carried out using a ChemiDoc MP Imaging System (Bio-Rad).

Strains, media and general methods: Strains used in this study are listed in **Table S4**, respectively. Yeast strains were cultured at 24°C either in rich media (YP - 1% yeast extract, 2% peptone, and 2% designated carbon source) or synthetic medium lacking specific amino acids, as indicated (8). New strains were constructed either by integrating a plasmid carrying a modified gene at an ectopic or native genomic locus or by crossing strains and isolating required meiotic progeny by tetrad analysis. Strains were sporulated at 24°C on medium containing 0.1% yeast extract, 0.05% glucose and 1% potassium acetate. Tetrad dissection and analysis were done as described (9). Yeast transformation, manipulation of *Escherichia coli*, and the preparation of bacterial growth media were performed as described previously (8). Protein extracts from G418-resistant meiotic progeny of transformants with tagged PCR products were assayed for the presence of the tagged protein by immunoblotting. The *Escherichia coli* strain DH5α was used to amplify all plasmids. Plasmids were purified from *E. coli* using the GenElute miniprep kit (Sigma-Aldrich). DH5α was grown in LB medium supplemented with ampicillin to select for plasmids. Restriction enzymes (Promega), DNA ligase (NEB), and high-fidelity DNA polymerase for PCR (Bio-Rad and Phenix) were used according to the manufacturer's instructions. For

Iodine tests in Figures S6D, plates were exposed to iodine vapor according to Chester (10). Strains used in this study are reported in **Table S4**.

Construction of the Cdc10-Glc7 chimera. The construction of the *CDC10-GLC7* fusion was described previously (11). The *GLC7-H65K* variant was introduced into pGEM-CDC10-GLC7 (pCZ6) using the QuikChange method. The *CDC10-GLC7* variant was subcloned as SacI/SpeI restriction fragments into the shuttle vector YCpIF16 (12) or the integration vector pMA1, which was made by cloning the *GAL1* promoter, including the HA epitope from YCpIF16, into the vector pRS306. The pMA1-*CDC10-GLC7* plasmid was linearized with NcoI prior to transformation into yeast and selection for uracil prototrophy.

*Induction of the Cdc10-Glc7 chimera for microscopy and immunoblotting***.** Stationary phase yeast cultures of strains with ectopically integrated *CDC10-GLC7* were prepared by growing cells in rich media (YP-raffinose) overnight (~16 hours) at 24°C on a rotor. The stationary phase cultures were diluted 1:20 in YP-raffinose and allowed to grow in a water bath shaker at 24°C for 3 hours, followed by addition of galactose to 2% final concentration. For experiments in which strains were transformed with plasmids containing *CDC10-GLC7* fusions, the same growth conditions and durations were used, except that transformants were grown in selective media to retain plasmids. Samples were taken simultaneously for microscopy and immunoblotting.

Microscopy: Aliquots of cultures (500µL) were centrifuged at 3000 rpm and the pelleted cells were pipetted on to a 2% agarose pad containing synthetic complete (SC) medium with 2% galactose. Cells were imaged using a Photometrics CoolSNAP HQ charge-coupled device camera or Prime95D CMOS camera through an Olympus UPlanFl 100 × /1.3 NA objective. Filters from Chroma Technology were used to image cells expressing proteins tagged with mCit. SlideBook 6 software (Intelligent Imaging Innovations) was used to control camera acquisition, fluorescence filter wheels, and the z axis stepping motor (Ludl Electronic Products). Images were acquired in a series of z-axis planes (0.5 µm apart). For quantification of fluorescence intensity of mCit-tagged proteins, images in nine planes were converted into a z-axis projection and the maximum fluorescence in 4 adjacent pixels was measured using ImageJ software. The number of cells containing Glc7-mCit foci were counted manually (n=300) and the nuclear-to-cytoplasmic fluorescence ratio was quantified by determining average intensity in nine adjacent pixels using ImageJ and plotted using Kaleidagraph.

Indirect immunofluorescence: The basic protocol and buffers used were as described in (13). In short, cultures were grown to mid-log phase in YP-Raffinose and HA-Cdc10-Glc7 was induced by adding galactose. Cells were fixed in 5% formaldehyde for 30 mins, followed by zymolyase treatment (20µg/ml) to remove the cell wall. Spheroplasted cells were incubated on poly lysine-coated slides, blocked and incubated in mouse monoclonal anti-HA 12CA5 antibody (1:2000 dilution) overnight in a petri dish lined with wet Kimwipes. After washing, cells were incubated in

a 1/500 dilution of Alexa 546-conjugated goat anti-mouse IgG (Sigma A-11003) for 1 hour. Finally, cells were stained with DAPI, covered with Fluoromount G mounting media (Thermo-Fisher Scientific), and images were acquired using the RFP filter set.

Immunoblot analysis: Immunoblotting was done as described in (14). Immunoblots were incubated with primary antibodies- rabbit polyclonal anti-GFP (JL-8) and mouse monoclonal anti-HA (12CA5) at 1:2000 and 1:1000 dilutions respectively, followed by incubating with HRP-conjugated secondary antibodies (Bio-Rad 170-5046 and 170-5047) and subsequent detection using ECL reagents (Clarity Western Bio-Rad). Protein levels were quantified from immunoblot signal using the ChemiDoc Touch imaging system with Image Lab 6.0 software (Bio-Rad). Anti-phosphoglycerate kinase (Pgk1) (Life Technologies) was used as a loading control.

Quantification and statistical analysis. SDS-PAGE and Western blots of PP1 coexpression pull-down studies were repeated 4 times (**Figure 1C**). All SPR and enzyme activity measurements were repeated between 3-9 times (described explicitly in **Tables 1, S2 and S3**); reported values are the average and standard deviation for the replicated measurements. Sigma Plot 12.5/13 or GraphPad Prism 7/8 was used for the statistical analysis of activity assays (**Figure 1D**; **Table S3).** Quantitative analysis of fluorescence in cells (SDS22-mCit) were performed as described (see Microscopy section in Methods); P-values calculated by two-tailed *t*-test (see **Figures 5D, 5H, S10B, S11B, S11C, S11F, S11G** and legends). All Western blots and microscopy experiments were performed at least three time using two biological replicates.

Data and software availability. Atomic coordinates and structure factors have been deposited in the Protein Data Bank (6OBN, 6OBP, 6OBQ, 6OBR, 6OBS and 6OBU). A compresensive summary of all resources used/generated in this study can be found in **Table S5**.

Table S1. ***Data collection and refinement statistics (1/2)***

	SDS22:PP1 coexpressed[a]	**SDS22:PP1 reconstituted[a]**	**PP1α H66K:MCLR[a]**
PDBID	6OBN	6OBP	6OBQ
Beamline	NSLS II 17-ID-2	SSRL 12-2	Home source
Wavelength (Å)	0.98	0.98	1.34
Data collection			
Space group	$P6_5\,2\,2$	$P2_1\,2_1\,2$	$P2_12_12_1$
Cell dimensions			
a, *b*, *c* (Å)	94.0, 94.0, 545.1	132.3, 69.7, 81.0	64.9, 76.6, 130.9
α, β, γ (°)	90, 90, 120	90, 90, 90	90, 90, 90
Resolution (Å)	29.87-2-70 (2.81-2.70)	38.73-2.70 (2.83-2.70)	22.04-1.84 (1.87-1.84)
R_{sym} or R_{merge}	0.175 (0.936)	0.112 (2.035)	0.14 (0.53)
I / σI	9.0 (2.2)	10.8 (1.8)	5.74 (1.82)
CC 1/2	0.997 (0.652)	0.998 (0.586)	0.992 (0.322)
Completeness (%)	99.5 (97.1)	99.2 (99.0)	99.9 (100.0)
Redundancy	8.5 (8.4)	7.4 (7.6)	7.80 (5.56)
Refinement			
Resolution (Å)	29.87-2.70 (2.77-2.70)	38.73-2.70 (2.84-2.70)	22.04-1.84 (1.87-1.84)
No. reflections	40847	20988	57317
R_{work} / R_{free}	0.20 (0.33)/0.25 (0.37)	0.21 (0.31)/0.20 (0.38)	0.23 (0.33)/0.26 (0.37)
No. atoms			
Protein	9351	4705	4709
Ligand/ion	77	14	144
Water	52	14	290
B-factors			
Protein	61.79	75.74	18.41
Ligand/ion	77.12	97.77	26.40
Water	46.16	65.40	22.28
R.m.s. deviations			
Bond lengths (Å)	0.006	0.002	0.003
Bond angles (°)	0.771	0.435	0.864
Ramachandran			
Outliers (%)	0.35	0.69	0.17
Allowed (%)	8.36	7.43	4.47
Favored (%)	91.30	91.88	95.36
Rotamer Outliers	2.48	4.37	0.78
Clashscore	5.39	4.66	4.01

[a]Data was collected from a single crystal

*Values in parentheses are for highest-resolution shell.

Data collection and refinement statistics (2/2)

	PP1α Y134A:MCLR[a]	**PP1α Y134K[a]**	**PP1α Y134K:MCLR[a]**
PDBID	6OBR	6OBS	6OBU
Beamline	SSRL 12-2	Home source	SSRL 9-2
Wavelength (Å)	0.98	1.34	0.98
Data collection			
Space group	$P2_12_12_1$	$P2_12_12_1$	$P2_12_12_1$
Cell dimensions			
a, *b*, *c* (Å)	64.9, 76.6, 131.2	65.1, 76.8, 131.6	65.4, 78.4, 134.0
α, β, γ (°)	90, 90, 90	90, 90, 90	90, 90, 90
Resolution (Å)	38.28-1.50 (1.52-1.50)	17.73-1.80 (1.83-1.80)	40.17-1.95 (2.00-1.95)
R_{sym} or R_{merge}	0.083 (1.127)	0.042 (0.489)	0.117 (0.925)
$I / \sigma I$	9.6 (1.7)	15.7 (2.4)	10.9 (1.7)
CC 1/2			
Completeness (%)	99.8 (97.9)	99.6 (95.0)	97.3 (80.3)
Redundancy	7.7 (7.3)	4.6 (2.7)	7.3 (4.6)
Refinement			
Resolution (Å)	38-28-1.50 (1.52-1.50)	17.73-1.80 (1.93-1.80)	40.17-1.95 (1.97-1.95)
No. reflections	105245	61204	49556
R_{work} / R_{free}	0.19 (0.31)/0.21 (0.34)	0.20 (0.36)/0.25 (0.38)	0.16 (0.29)/0.20 (0.32)
No. atoms			
Protein	4726	4666	4730
Ligand/ion	148	20	193
Water	349	505	342
B-factors			
Protein	28.79	21.53	25.92
Ligand/ion	32.14	30.50	40.41
Water	35.48	30.36	33.57
R.m.s. deviations			
Bond lengths (Å)	0.015	0.010	0.009
Bond angles (°)	0.917	0.818	0.900
Ramachandran			
Outliers (%)	0.17	0.00	0.00
Allowed (%)	3.61	4.47	3.09
Favored (%)	96.21	95.53	96.91
Rotamer Outliers (%)	0.59	0.79	0.97
Clashscore	2.73	3.24	3.21

[a]Data was collected from a single crystal

*Values in parentheses are for highest-resolution shell.

Table S2: ***SPR binding kinetics for the association of NIPP1^ with PP1 variants***

PP1 variant	k_{on} (M^{-1} s^{-1})‡	k_{off} (s^{-1})‡	K_D (nM)‡	χ^{2}‡	*n*
No metal*					
PP1α 7-330	$9.27x10^5 \pm 1.22x10^5$	$2.15x10^{-2} \pm 1.4x10^{-3}$	23.5 ± 3.4	0.20 ± 0.06	5
PP1γ 7-323	$1.34x10^6 \pm 9.29x10^4$	$3.10x10^{-2} \pm 6.9x10^{-3}$	23.1 ± 3.7	0.48 ± 0.18	3
PP1α 7-300	$6.14x10^5 \pm 4.44x10^4$	$4.98x10^{-2} \pm 5.3x10^{-3}$	81.6 ± 12.3	0.34 ± 0.06	4
PP1α 7-300 Y134A	$6.75x10^5 \pm 1.43x10^5$	$5.94x10^{-2} \pm 1.00x10^{-2}$	91.3 ± 25.6	0.36 ± 0.20	4
PP1α 7-300 Y134F	$6.73x10^5 \pm 9.20x10^4$	$3.65x10^{-2} \pm 4.0x10^{-3}$	54.7 ± 6.6	0.55 ± 0.11	5
PP1α 7-300 Y134K	$6.81x10^5 \pm 1.69x10^5$	$5.34x10^{-2} \pm 1.74x10^{-2}$	83.7 ± 36.2	0.19 ± 0.07	4
PP1α 7-300: MC	$1.42x10^6 \pm 1.48x10^5$	$6.72x10^{-3} \pm 4x10^{-4}$	4.8 ± 0.3	0.96 ± 0.59	4
PP1α 7-300 H66K	$8.47x10^5 \pm 6.46x10^4$	$5.3x10^{-2} \pm 5x10^{-4}$	70.3 ± 5.1	0.42 ± 0.02	3
with Mn^{2+}					
PP1α 7-330	$1.18x10^6 \pm 6.50x10^4$	$1.90x10^{-2} \pm 1.5x10^{-3}$	16.0 ± 4.8	0.48 ± 0.15	4
PP1γ 7-323	$1.03x10^6 \pm 3.61x10^4$	$2.15x10^{-2} \pm 1.2x10^{-3}$	21.0 ± 1.7	0.24 ± 0.11	3
PP1α 7-300	$8.32x10^5 \pm 1.59x10^5$	$3.94x10^{-2} \pm 3.0x10^{-3}$	48.7 ± 8.8	0.76 ± 0.25	6
PP1α 7-300 Y134A	$5.60x10^5 \pm 9.09x10^4$	$5.14x10^{-2} \pm 6.7x10^{-3}$	93 ± 11.9	0.85 ± 0.46	4
PP1α 7-300 Y134F	$6.72x10^5 \pm 1.09x10^5$	$3.85x10^{-2} \pm 2.4x10^{-3}$	58.3 ± 8.5	0.23 ± 0.15	6
PP1α 7-300 Y134K	$7.92x10^5 \pm 6.65x10^4$	$5.69x10^{-2} \pm 3.9x10^{-3}$	72.0 ± 4.4	0.45 ± 0.12	4
PP1α 7-300: MC	$1.31x10^6 \pm 7.85x10^4$	$7.05x10^{-3} \pm 1.1x10^{-3}$	5.4 ± 1.1	0.50 ± 0.06	4
PP1α 7-300 H66K	$7.33x10^5 \pm 1.20x10^5$	$4.66x10^{-2} \pm 9x10^{-4}$	64.4 ± 8.5	0.79 ± 0.14	3
with Zn^{2+}					
PP1α 7-330	$6.37x10^5 \pm 2.10x10^5$	$1.72x10^{-2} \pm 3.3x10^{-3}$	27.8 ± 5.1	0.15 ± 0.08	3

^$NIPP1_{158-216}$; these SPR experiments serve as controls to show that the absence of metal in the SPR buffer does impact NIPP1 binding (which binds PP1 distally from the active site).

Table S3: ***T_ms and Michalis-Menten activity constants of PP1 variants***

PP1 variant	T_m (°C)	*n*	k_{cat} (s^{-1})	K_m	*n*
PP1, *wt variants*					
$PP1\alpha_{7-300}$	75.1 ± 0.2	3	1.051 ± 0.012	742.6 ± 24.8	9
$PP1\gamma_{7-323}$	75.0 ± 0.1	3	0.795 ± 0.014	518.8 ± 29.7	9
$PP1\alpha_{1-300}$	75.8 ± 0.1	3	0.887 ± 0.022	717.8 ± 50.8	6
$PP1\alpha_{7-330}$	76.2 ± 0.2	3	0.878 ± 0.009	712.5 ± 20.7	6
$PP1\alpha_{7-300}$:MC	81.4 ± 0.5	3	*no activity*	*no activity*	3
$PP1\alpha_{7-330}$:MC	81.9 ± 0.7	3	*no activity*	*no activity*	3
PP1, *M1 metal binding variants*					
$PP1\alpha_{7-300}$D64A	Unfolded		-	-	
$PP1\alpha_{7-300}$H66K	68.3 ± 0.1	3	*no activity*	*no activity*	6
PP1, *CASINRIYG loop variants*					
$PP1\alpha_{7-300}$Y134A	76.0 ± 0.2	3	0.013 ± 0.001	102.1 ± 20.4	6
$PP1\alpha_{7-300}$Y134A:MC	75.1 ± 0.1	3	*no activity*	*no activity*	3
$PP1\alpha_{7-300}$Y134K	74.4 ± 0.1	3	0.004 ± 0.001	219.2 ± 182.5	9
$PP1\alpha_{7-300}$G135A	Unfolded		-	-	
$PP1\alpha_{7-300}$Y134F	73.2 ± 0.2	3	0.720 ± 0.008	557.8 ± 23.5	3

Table S4: ***Yeast strains used in this study***

Yeast strain #	Description	Source
KT1112	*MAT**a** leu2 his3 ura3-52*	(15)
KT1113	*MATα leu2 his3 ura3-52*	(16)
KT2420	*MAT **a** GLC7-mCitrine::SpHis5*	(14)
KT2492	*MAT α GLC7-mCitrine::SpHis5*	This study
KT2762	*MAT α SDS22-mCitrine::SpHis5 bin4Δ::NatMX*	This study
KT2764	*MATα SDS22-mCitrine::SpHis5*	This study
KT2926	*MATα pGAL1-CDC10-GLC7::URA3 SDS22-mCitrine::SpHis5 bin4Δ::NatMX*	This study
KT2947	*MATα pGAL1-CDC10-GLC7^{H65K}::URA3 SDS22-mCitrine::SpHis5 bin4Δ::NatMX*	This study
KT2954	*MAT**a** pGAL1-CDC10-GLC7::URA3 YPI1-mCitrine::SpHis5 bin4Δ::NatMX*	This study
KT2986	*MAT**a** pGAL1-CDC10-GLC7^{H65K}::URA3 YPI1-mCitrine::SpHis5 bin4Δ::NatMX*	This study
KT4020 X KT4021	*MATα/a pGAL1-CDC10-GLC7^{H65K}::URA3 SDS22-mCitrine::SpHis5 bin4Δ::NatMX GIP3-mCherry::SpHis5*	This study
KT4022 X KT4023	*MATα/a pGAL1-CDC10-GLC7::URA3 SDS22-mCitrine::SpHis5 bin4Δ::NatMX GIP3-mCherry::SpHis5*	This study
KT4038	*MAT**a** pGAL1-CDC10-GLC7::URA3 SDS22-mCitrine::SpHis5*	This study
KT4097	*MATα pGAL1-CDC10-GLC7^{Y133A}::URA3 SDS22-mCitrine::SpHis5 bin4Δ::NatMX*	This study
KT4110	*MATα pGAL1-CDC10-GLC7$^{K146A\ K149A}$::URA3 SDS22-mCitrine::SpHis5 bin4Δ::NatMX*	This study

All yeast strains are congenic to KT1113 and KT1112 (*leu2 his3 ura3-52*).

Table S5: ***Key resources***

REAGENT or RESOURCE	SOURCE	IDENTIFIER
Antibodies		
Primary antibody: rabbit polyclonal anti-PP1γ (PA5-21671)	Thermo Fisher Scientific	Cat#PA5-21671
Primary antibody: rabbit polyclonal anti-GFP (JL-8)	Babu et al. J. Cell Sci. 115:4957-4968 (2002)	N/A
Primary antibody: mouse monoclonal anti-HA (12CA5)	Wilson et al. Cell 37: 767-778 (1984)	N/A
Primary antibody: mouse monoclonal anti-PGK1 (22C5D8)	Thermo Fisher Scientific, formerly Life Technologies	Cat#459250
Secondary antibodies: Immun-Star (GAM)-HRP conjugated	Bio-Rad	Cat#170-5047 (mouse) Cat#170-5046 (rabbit)
Rabbit IgG StarBright B520	Bio-Rad	Cat#12005870
Alexa 546-conjugated goat anti-mouse IgG	Sigma Aldrich	Cat#A11003
Bacterial and Virus Strains		
E. coli BL21-Gold (DE3)	Agilent	Cat#230132
E.coli BL21 (DE3) RIL expression strain	Agilent	Cat#230245
E.coli XL1-Blue Competent Cells	Agilent	Cat #200249
E. coli DH5α	Thermo Fisher Scientific	Cat#18258012
Chemicals, Peptides, and Recombinant Proteins		
Microcystin-LR	Enzo Life Sciences	Cat#ALX-350-012-C500
Li-COR Odyssey Blocking Buffer	Li-COR Biosciences	Cat#927-40000
Gibco Expi293 Expression medium	Thermo Fisher Scientific	Cat#A1435102
Opti-MEM Reduced serum medium	Thermo Fisher Scientific	Cat#31985062
Expifectamine 293 transfection reagents	Thermo Fisher Scientific	Cat#A14525
FectoPro	Polyplus	Cat#116-040
Isopropyl-b-D-1-thiogalactoside (IPTG)	BioSynth	Cat#I-8020
Phusion High-Fidelity DNA polymerase	Thermo Scientific	Cat#F-530L
Triton X-100	MERCK	Cat#1.08603
Dithiothreitol (DTT)	COLDBIO	Cat#DTT100
TECP	GOLDBIO	Cat#TCEP1
Protease inhibitor cocktail tablets, c0mplete, EDTA free	Roche	Cat#05056489001
Adenosine 5′-triphosphate (ATP) disodium salt hydrate	Sigma Aldrich	Cat#A3377
Magnesium chloride hexahydrate	ACROS Organics	Cat#AC197530010
PNPP Substrate	Thermo Scientific	Cat#34045
PEG 4000	Sigma Aldrich	Cat#8074901000
2-methyl-2,4-pentanediol (MPD)	Sigma Aldrich	Cat#68338
Sodium phosphate monobasic	Fisher Scientific	Cat#BP330-500
Potassium phosphate dibasic	Fisher Scientific	Cat#AC215472500
Tween 20	Fisher Scientific	Cat#BP337
Fluoromount-G mounting media	Thermo Fisher Scientific	Cat#00-4958-02
TEV (Tobacco Etch Virus) protease	This paper	N/A
Clarity™ Western ECL substrate	Bio-Rad	Cat#1705060
Critical Commercial Assays		
QuikChange II site-directed	Agilent	Cat#200523
GenElute miniprep kit	Sigma Aldrich	Cat#PLN70

Plasmid DNA Mini kit - Classic	Zymo Research	Cat#D4015
PureLink HiPure Plasmid Maxiprep kit	Thermo Fisher Scientific	Cat#K210007
Zymoclean Gel DNA Recovery kit	Zymo Research	Cat#D4007
LMB crystallization screen	Molecular Dimensions	Cat#MD1-98
Deposited Data		
Atomic coordinates, co-expressed SDS22$_{56-360}$:PP1α$_{1-300}$ complex	This paper	PDB: 6OBN
Atomic coordinates, re-constituted SDS22$_{56-360}$:PP1α$_{1-300}$ complex	This paper	PDB: 6OBP
Atomic coordinates, PP1α$_{7-300}$ H66K in complex with microcystin-LR	This paper	PDB: 6OBQ
Atomic coordinates, PP1α$_{7-300}$ Y134A in complex with microcystin-LR	This paper	PDB:6OBR
Atomic coordinates, PP1α$_{7-300}$ Y134K	This paper	PBD: 6OBS
Atomic coordinates, PP1α$_{7-300}$ Y134K in complex with microcystin-LR	This paper	PDB: 6OBU
Experimental Models: Cell Lines		
Expi293F	Thermo Fisher Scientific	Cat#A14527
Yeast Strains: KT1112- *MAT**a** leu2 his3 ura3-52* KT1113- *MATα leu2 his3 ura3-52* KT2420- *MAT **a** GLC7-mCitrine::SpHis5* KT2492- *MAT α GLC7-mCitrine::SpHis5* KT2762- *MAT α SDS22-mCitrine::SpHis5 bin4Δ::NatMX* KT2764- *MAT α SDS22-mCitrine::SpHis5* KT2926- *MAT α pGAL1-CDC10-GLC7::URA3 SDS22-mCitrine::SpHis5 bin4Δ::NatMX* KT2947- *MAT α pGAL1-CDC10-GLC7$_{H65K}$::URA3 SDS22-mCitrine::SpHis5 bin4Δ::NatMX* KT4038- *MAT **a** pGAL1-CDC10-GLC7::URA3 SDS22-mCitrine::SpHis5* KT4097- *MAT α pGAL1-CDC10-GLC7$_{Y133A}$::URA3 SDS22-mCitrine::SpHis5 bin4Δ::NatMX* KT4110- *MAT α pGAL1-CDC10-GLC7$_{K146A\ K149A}$::URA3 SDS22-mCitrine::SpHis5 bin4Δ::NatMX* KT4020 X KT4021- *MAT α/a pGAL1-CDC10-GLC7$_{H65K}$::URA3 SDS22-mCitrine::SpHis5 bin4Δ::NatMX GIP3-mCherry::SpHis5* KT4022 X KT4023- *MAT α/a pGAL1-CDC10-GLC7::URA3 SDS22-mCitrine::SpHis5 bin4Δ::NatMX GIP3-mCherry::SpHis5*	 Stuart JS et al, *Mol Cell Biol* 14(2):896–905 (1996) Frederick DL et al, *Mol Cell Biol* 16(6):2922–2931 (1994) Ravindran et al., 2018 This study This study This study This study This study This study This study This study This study	N/A
Recombinant DNA		
pRP1B PP1α$_{1-300}$ WT (Human PP1α 1-300)	This paper	N/A
pRP1B PP1α$_{7-300}$ WT (Human PP1α 7-300)	This paper	N/A
pRP1B PP1α$_{7-300}$ H66K (Human PP1α 7-300, H66K)	This paper	N/A
pRP1B PP1α$_{7-300}$ Y134F (Human PP1α 7-300, Y134F)	This paper	N/A
pRP1B PP1α$_{7-300}$ Y134A (Human PP1α 7-300, Y134A)	This paper	N/A

pRP1B PP1α$_{7-300}$ Y134K (Human PP1α 7-300, Y134K)	This paper	N/A
pRP1B PP1α$_{7-300}$ G135A (Human PP1α 7-300, G135A)	This paper	N/A
pRP1B PP1α$_{7-300}$ D64A (Human PP1α 7-300, D64A)	This paper	N/A
pET_M30_MBP NIPP1$_{158-216}$ (Human NIPP1 158-216)	O'Connell, et al. Structure 20:1746-1756 (2012)	N/A
pcDNA3.4_K_RP1B SDS22$_{56-360}$ (Human SDS22 56-360)	This paper	N/A
pcDNA3.4_K_RP1B PP1α$_{1-300}$ (Human PP1α 1-300)	This paper	N/A
pcDNA3.4_K_RP1B I-2$_{9-165}$ (Human Inhibitor-2 9-165)	This paper	N/A
pcDNA3.4_K_RP1B I-3$_{1-126}$ (Human Inhibitor-3 1-126)	This paper	N/A
pcDNA3.4_K_RP1B Spinophilin$_{417-602}$ (Rat Spinophilin 417-602)	This paper	N/A
pGEM-CDC10-GLC7 (pCZ6)	Larson, J. R et al, *Mol. Biol. Cell* **29**, 3040-3051 (2008)	N/A
YCp-IF16 CDC10-GLC7::TRP (pJL187)	This study	N/A
YCP-IF16 CDC10-glc7^{H65K}::TRP (pJL195)	This study	
YEp-lac195 SDS22-myc::URA (YEpEGP1myc- High Copy Sds22)	Hisamoto, N et al, *Mol. Cell. Biol.* **15**, 3767-3776 (1995)	N/A
Software and Algorithms		
SPR Autolink	Reichert Inc	http://www.reichert.com
TraceDrawer	Ridgeview Instruments AB	http://www.ridgeview.eu/software/tracedrawer
CLAMP	Myszka, et al., 1998	https://doi.org/10.1016/S0968-0004(98)01183-9; note – this software isn't commercially available any longer, we obtained it from Reichert during install.
Scrubber	BioLogic Software	http://www.biologic.com.au/scrubber.html
SigmaPlot 12.5/13	Systat software	https://systatsoftware.com/
PHENIX	Adams et al., 2010	https://www.phenix-online.org/
WinCoot	Emsley et al., 2004	http://www2.mrc-lmb.cam.ac.uk/personal/pemsley/coot/
PYMOL	Schrodinger, LLC	https://www.pymol.org
XDS	Kabsch, 2010	http://xds.mpimf-heidelberg. mpg.de/
PROTEUM 3	Bruker	https://www.bruker.com/

GraphPad Prism 8	GraphPad	https://www.graphpad.com/scientific-software/prism/
ImageJ	Schneider et al., 2012	https://imagej.nih.gov
Image Lab	Bio-Rad	http://www.bio-rad.com/en-us/product/image-lab-software?ID=KRE6P5E8Z
Slidebook	Intelligent Imaging Innovations, Inc.	https://www.intelligent-imaging.com/slidebook
Other		
SPR Sensorchip	Xantec bioanalytics, GmbH	Cat#NiD50L
Prime 95B Camera	Teledyne Photometrics	https://www.photometrics.com/products/scmos/prime95B

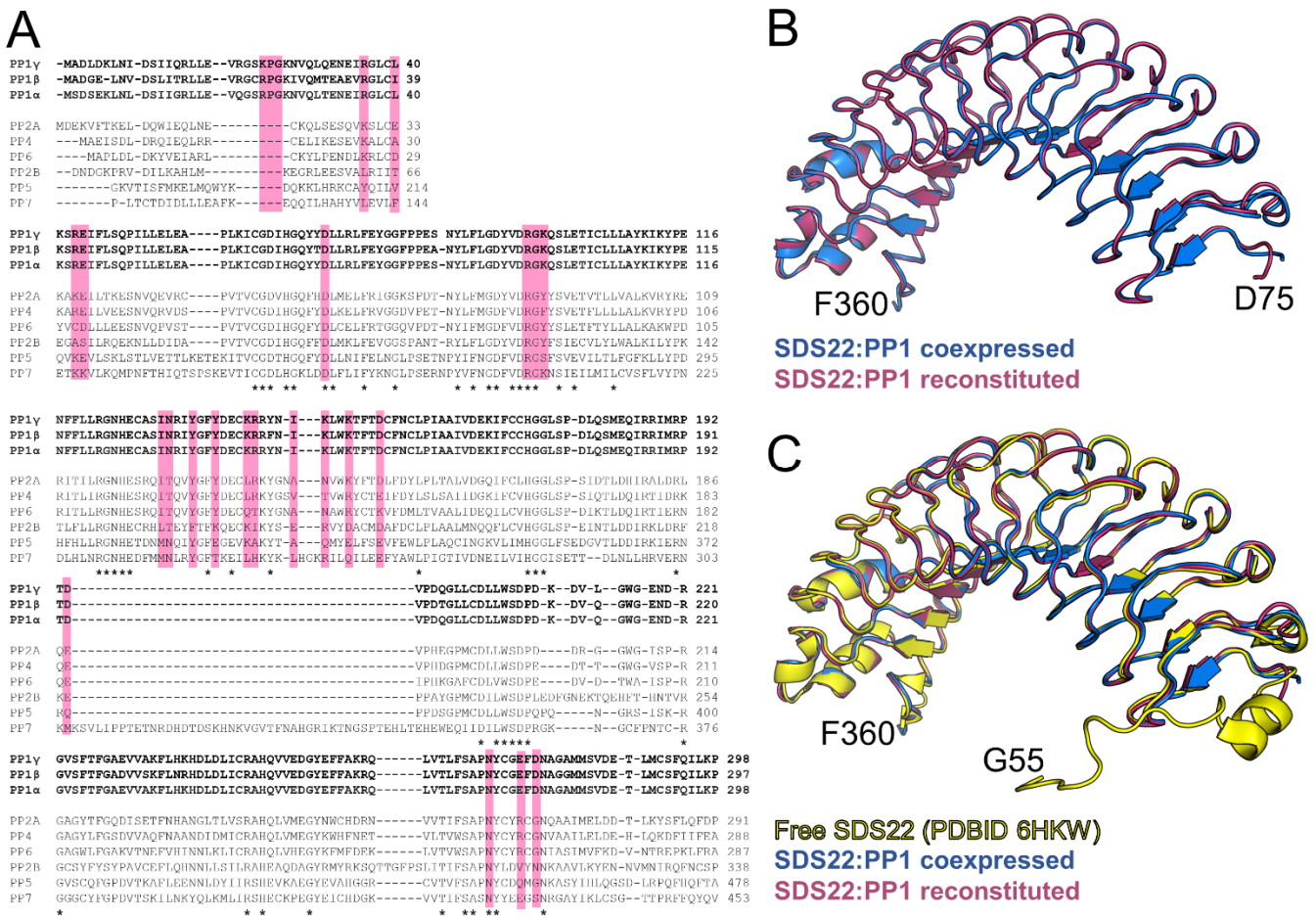

Figure S1. ***Sequence alignment of the PPP family and SDS22 structure***. **A**. Sequence alignment of the PPP family illustrates the lack of conservation in the PP1 residues that comprise the SDS22:PP1 interface (highlighted magenta). Asterisk (*) indicates fully conserved residues. **B**. Cartoon showing the overlay of the crystal structures of SDS22 from the coexpressed (blue) and reconstituted (pink) SDS22:PP1 complexes. **C**. Same as B except the overlay includes the crystal structure of free SDS22 (PDBID 6HKW, yellow). RMDS for the overlays are the following: SDS22 from the coexpressed SDS22:PP1 complex (RMSD=0.47 Å compared with free SDS22); SDS22 from the reconstituted SDS22:PP1 complex (RMSD=0.44 Å compared with free SDS22).

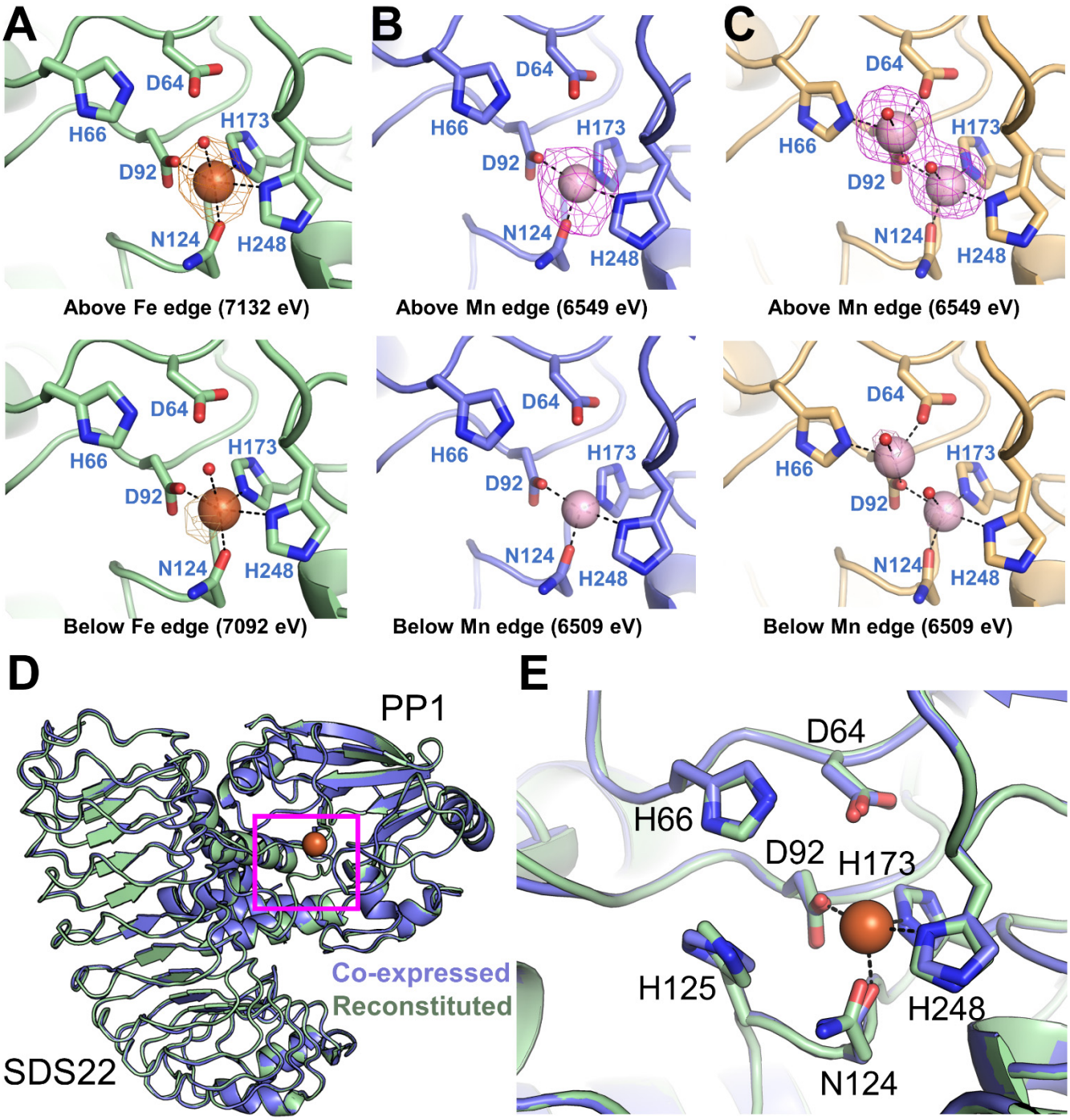

Figure S2. ***PP1 active site metals differ in otherwise identical SDS22:PP1 reconstituted versus coexpressed complexes.*** **A.** *Coexpressed SDS22:PP1 complex (PP1 expressed in mammalian cells)*. Anomalous map from data collected just above (7132 eV; above) and just below (7092 eV; bottom) the Fe absorption edge indicates the presence of a single Fe^{2+} at the M2 position of the active site. Orange mesh, anomalous map of Fe at 4σ; orange spheres are Fe^{2+}. **B.** *Reconstituted SDS22:PP1 (PP1 expressed in E. coli)*. Anomalous map from data collected just above (6549 eV) and just below (6509 eV) the Mn^{2+} absorption edge indicates the

presence of a single atom of Mn^{2+} at the M2 position of the active site. Pink mesh, anomalous map of Mn^{2+} at 4σ; pink spheres, Mn^{2+}. **C.** *$PP1_{Y134A}$ (expressed in E. coli)*. Anomalous map from data collected just above (6549 eV) and just below (6509 eV) the Mn^{2+} absorption edge indicates the presence Mn^{2+} ion at both the M1 and M2 positions. Pink mesh, anomalous map of Mn^{2+} at 4σ; pink spheres, Mn^{2+}. **D**. Overlay of the crystal structures of coexpressed (lavender) and reconstituted (green) SDS22:PP1 show that the coexpressed and reconstituted SDS22:PP1 complexes are identical. Magenta box is the region shown in 'B'. **E**. Close up of the PP1 active sites in both complexes. Metal coordination residues are shown as sticks; orange sphere, Fe^{2+} at the active site of coexpressed SDS22:PP1 (Mn^{2+} in reconstituted SDS22:PP1; not shown but located at same position as the Fe^{2+} ion).

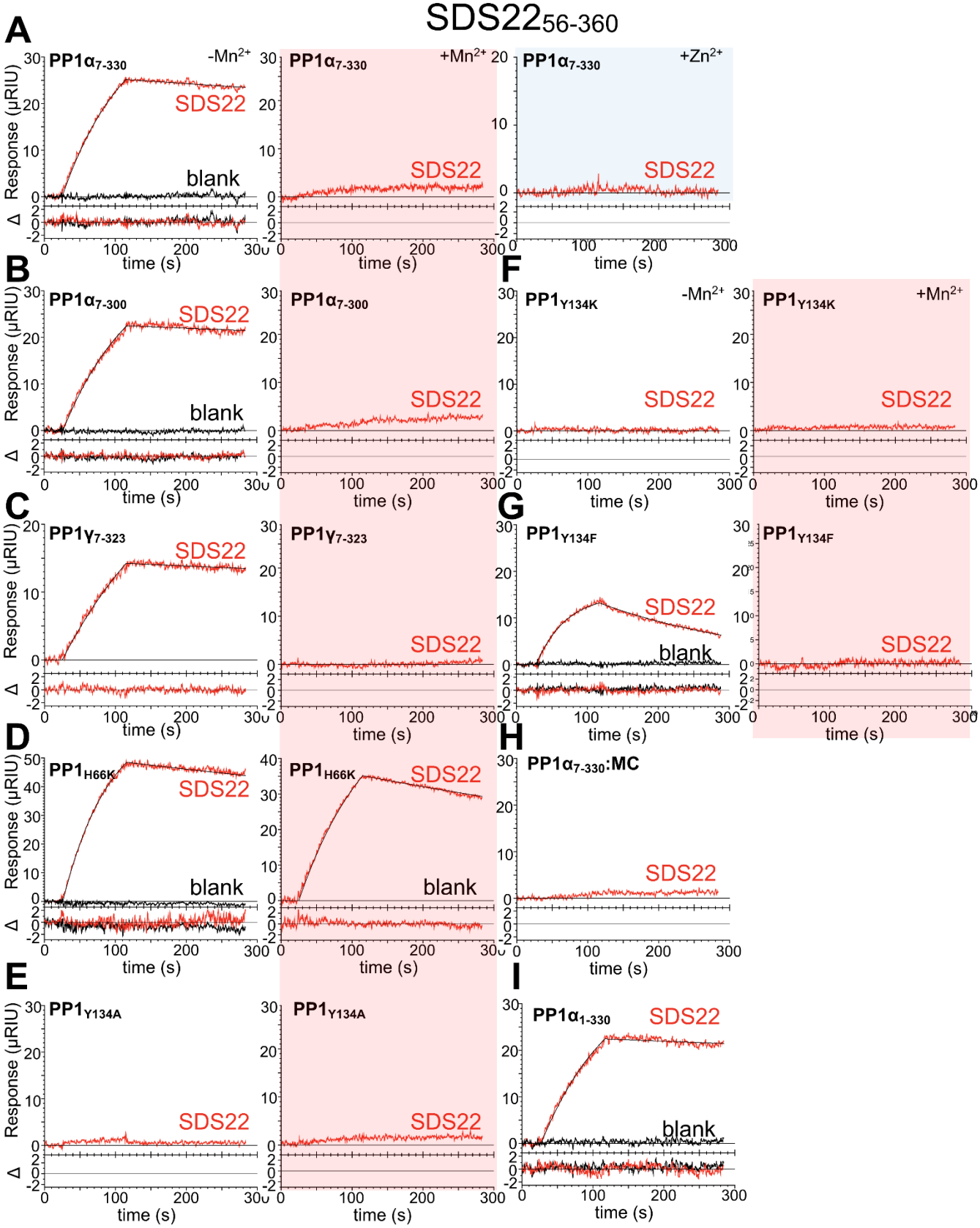
SDS22$_{56-360}$
A
PP1α$_{7-330}$
-Mn^{2+}
+Mn^{2+}
+Zn^{2+}
SDS22
blank
B
PP1α$_{7-300}$
C
PP1γ$_{7-323}$
D
PP1$_{H66K}$
E
PP1$_{Y134A}$
F
PP1$_{Y134K}$
G
PP1$_{Y134F}$
H
PP1α$_{7-330}$:MC
I
PP1α$_{1-330}$
Response (μRIU)
Δ
time (s)

Figure S3. ***SPR sensorgrams for SDS22 and PP1 variants*.** SPR sensorgrams depicting $SDS22_{56-360}$ (red) binding to PP1 constructs in the absence (white background) and presence of $MnCl_2$ (pink background) or $ZnCl_2$ (blue background). **A**. $PP1\alpha_{7-330}$. **B**. $PP1\alpha_{7-300}$, **C**. $PP1\gamma_{7-323}$. **D**. $PP1_{H66K}$. **E**. $PP1_{Y134A}$. **F**. $PP1_{Y134K}$. **G**. $PP1_{Y134F}$. **H**. $PP1\alpha_{1-300}$. **I**. $PP1\alpha_{7-330}$:MC. Concentration of injected SDS22 is 500 nM. When binding data is fit with a kinetic model (one-to-one), a plot of the residuals is shown below each trace.

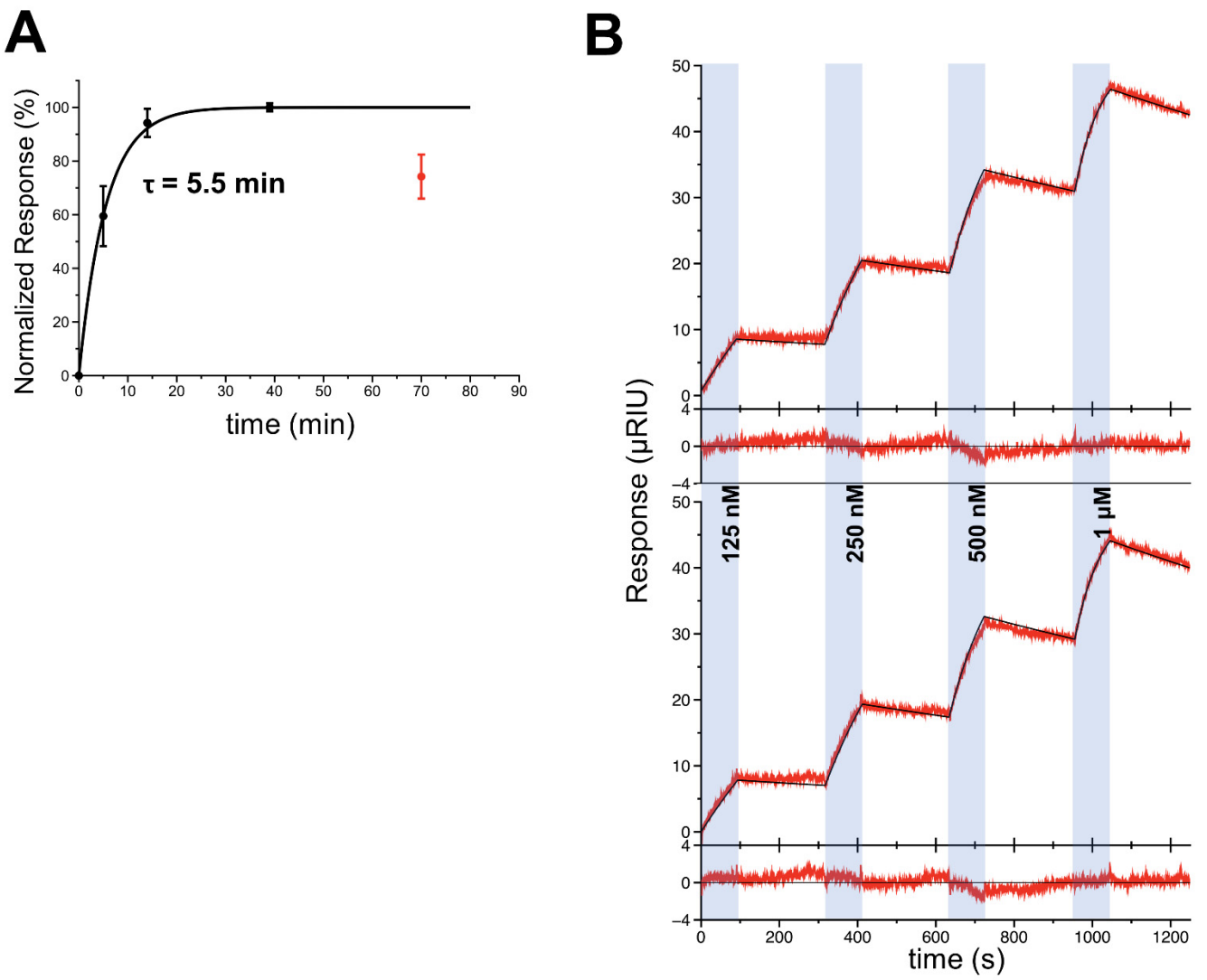

Figure S4. ***Time-course of M1 metal loss in PP1 and SDS22 binding to M1-metal free PP1***. **A**. The normalized maximum response of SDS22 binding to PP1α$_{7\text{-}300}$ was measured at increasing incubation times in the absence of Mn^{2+}. An increase in SDS22 binding to PP1 was observed over the course of 40 minutes and a drop in signal was observed at 70 minutes (red time point). Data were fit using a one-phase association model excluding the 70 minute time point to determine the M1 half-life. **B**. SPR sensorgrams showing duplicate kinetic titrations of SDS22$_{56\text{-}360}$ binding to PP1α$_{7\text{-}330}$.

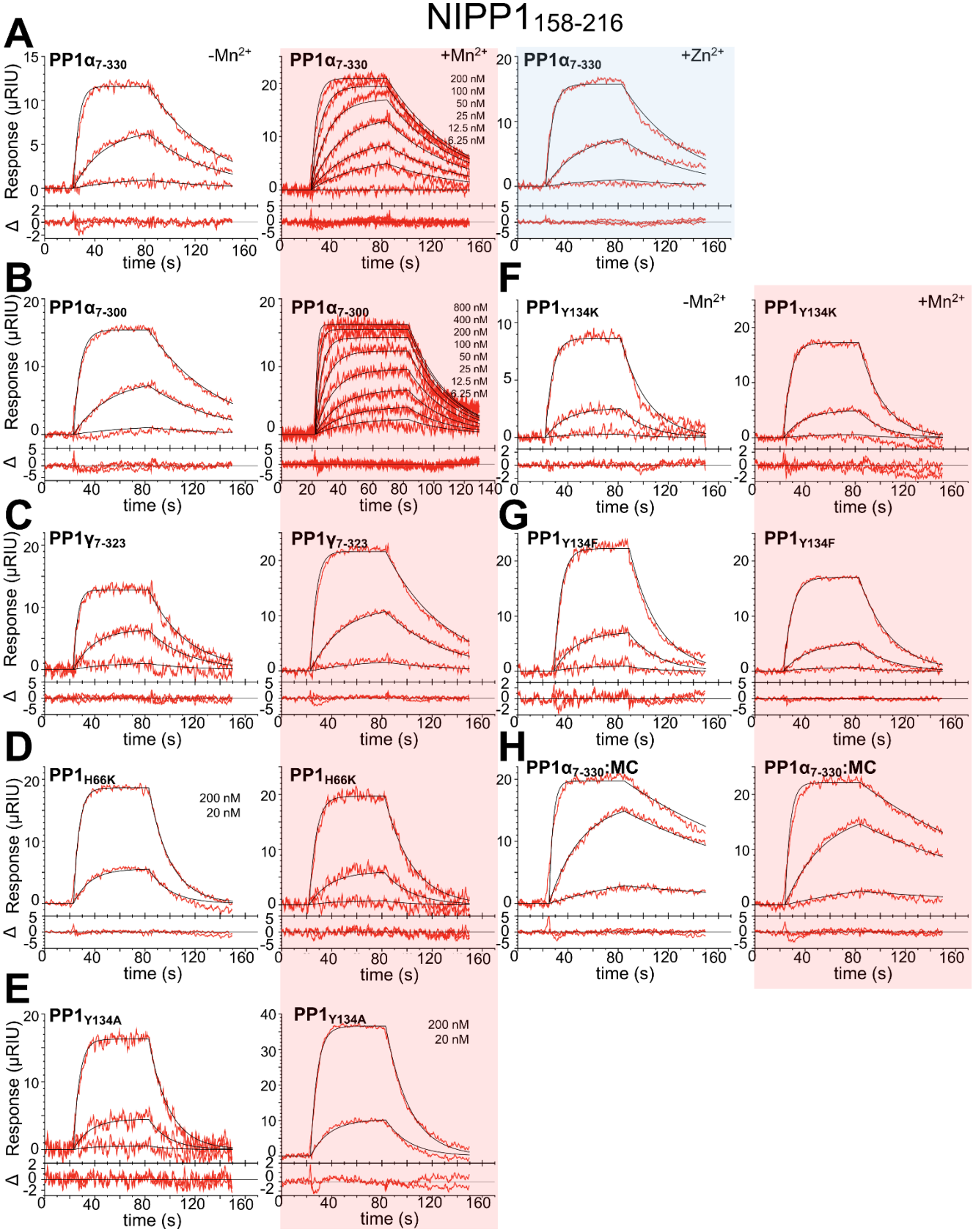
NIPP1158-216
A
PP1α7-330
-Mn2+
+Mn2+
+Zn2+
200 nM
100 nM
50 nM
25 nM
12.5 nM
6.25 nM
B
PP1α7-300
800 nM
400 nM
200 nM
100 nM
50 nM
25 nM
12.5 nM
6.25 nM
C
PP1γ7-323
D
PP1H66K
200 nM
20 nM
E
PP1Y134A
200 nM
20 nM
F
PP1Y134K
-Mn2+
+Mn2+
G
PP1Y134F
H
PP1α7-330:MC
Response (μRIU)
Δ
time (s)

Figure S5. ***SPR sensorgrams NIPP1 and PP1 variants.*** SPR sensorgrams measuring the binding of $NIPP1_{158-216}$ (control, a known PP1 binding regulator) to PP1 variants in the absence (white background) or presence of $MnCl_2$ (pink background) or $ZnCl_2$ (blue background). **A**. $PP1\alpha_{7-330}$. **B**. $PP1\alpha_{7-300}$. **C**. $PP1\gamma_{7-323}$. **D**. $PP1_{H66K}$. **E**. $PP1_{Y134A}$. **F**. $PP1_{Y134K}$. **G**. $PP1_{Y134F}$. **H**. $PP1\alpha_{7-330}$:MC. Concentrations of injected $NIPP1_{158-216}$ are 2 nM, 20 nM and 200 nM unless otherwise specified. When binding data is fit with a kinetic model (one-to-one), a plot of the residuals is shown below each trace.

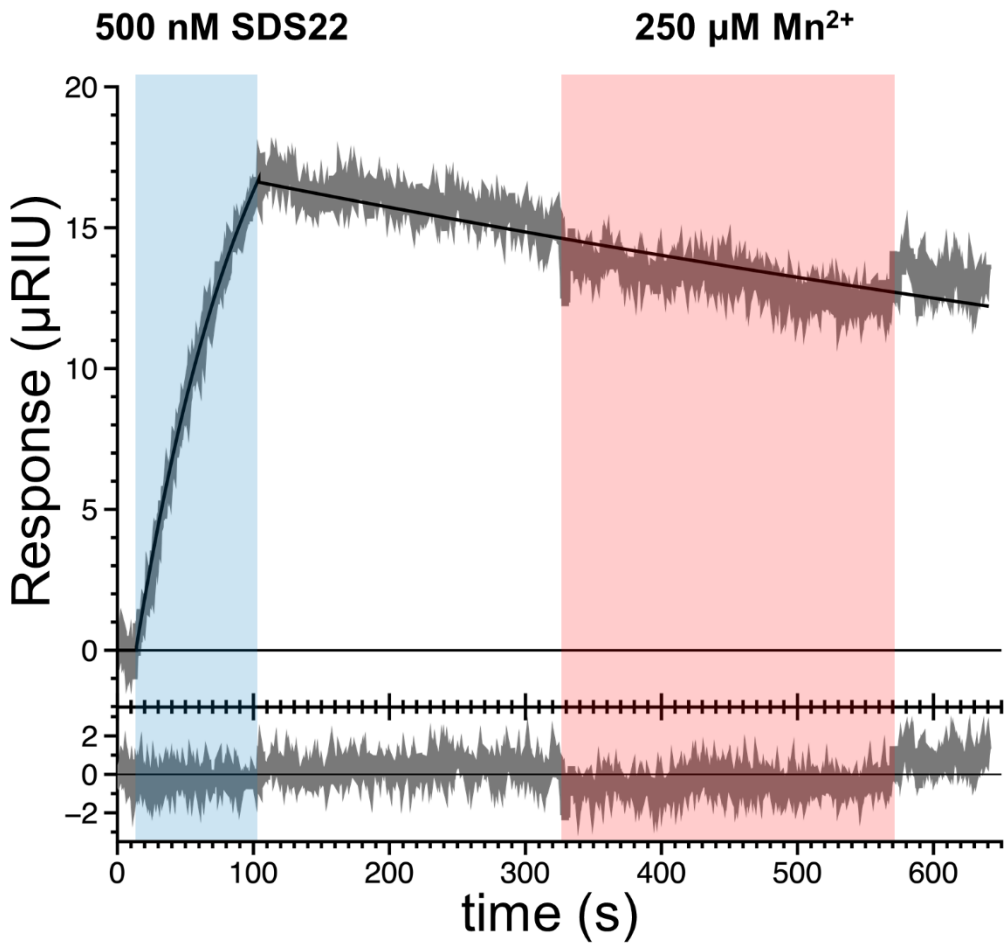

Figure S6. ***Mn^{2+} is unable to dissociate assembled SDS22:PP1 complexes.*** A representative SPR sensorgram depicting SDS22 (blue) injected onto a surface charged with PP1 ($PP1\alpha_{7\text{-}330}$). After 3 minutes of flow in the absence of SDS22, 250 μM $MnCl_2$ (red) was injected onto the SDS22-PP1 complex surface for four minutes. During this time, no changes in the rate of dissociation of SDS22 from PP1 were observed. This shows that the presence of metals not sufficient to dissociate SDS22 from PP1.

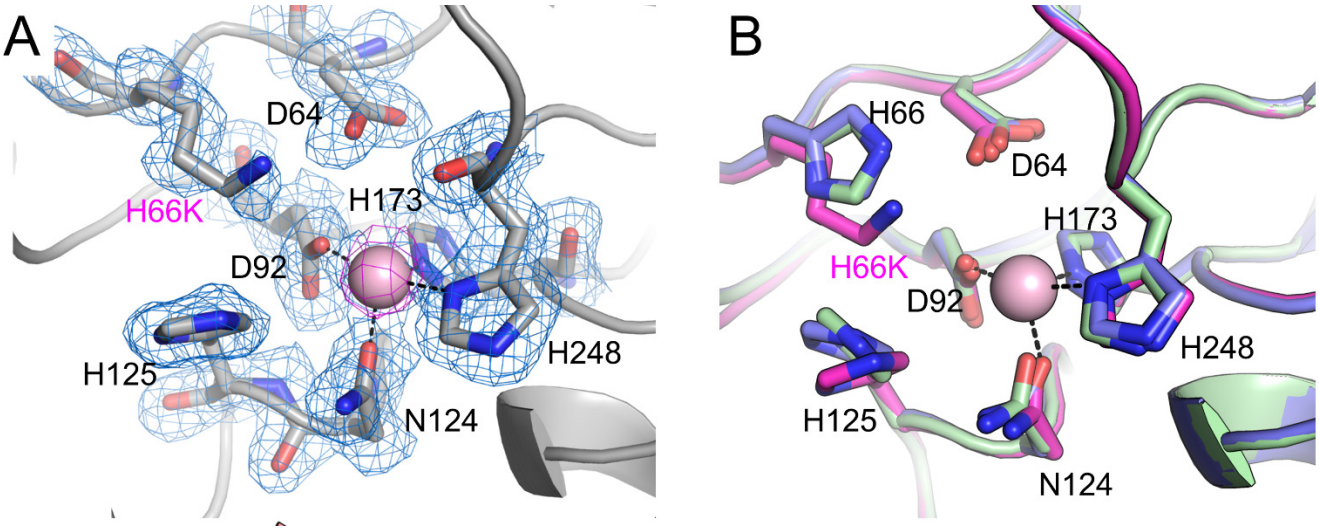

Figure S7. ***Crystal structure of the H66K variants***. **A**. Crystal structure of $PP1_{H66K}$ has only a single metal present at the active site (in position M2; anomalous map (magenta mesh; contoured at 4.0 σ) from data collected just above (6549 eV) and just below (6509 eV) the Mn^{2+} absorption edge indicates the presence of a single atom of Mn^{2+}). Blue mesh, $2F_o$-F_c map, contoured at 1.0 σ. Pink sphere, Mn^{2+} ion. **B**. Overlay of the active sites of $PP1_{H66K}$ (magenta) with coexpressed SDS22:PP1 (lavender) and reconstituted SDS22:PP1 (green).

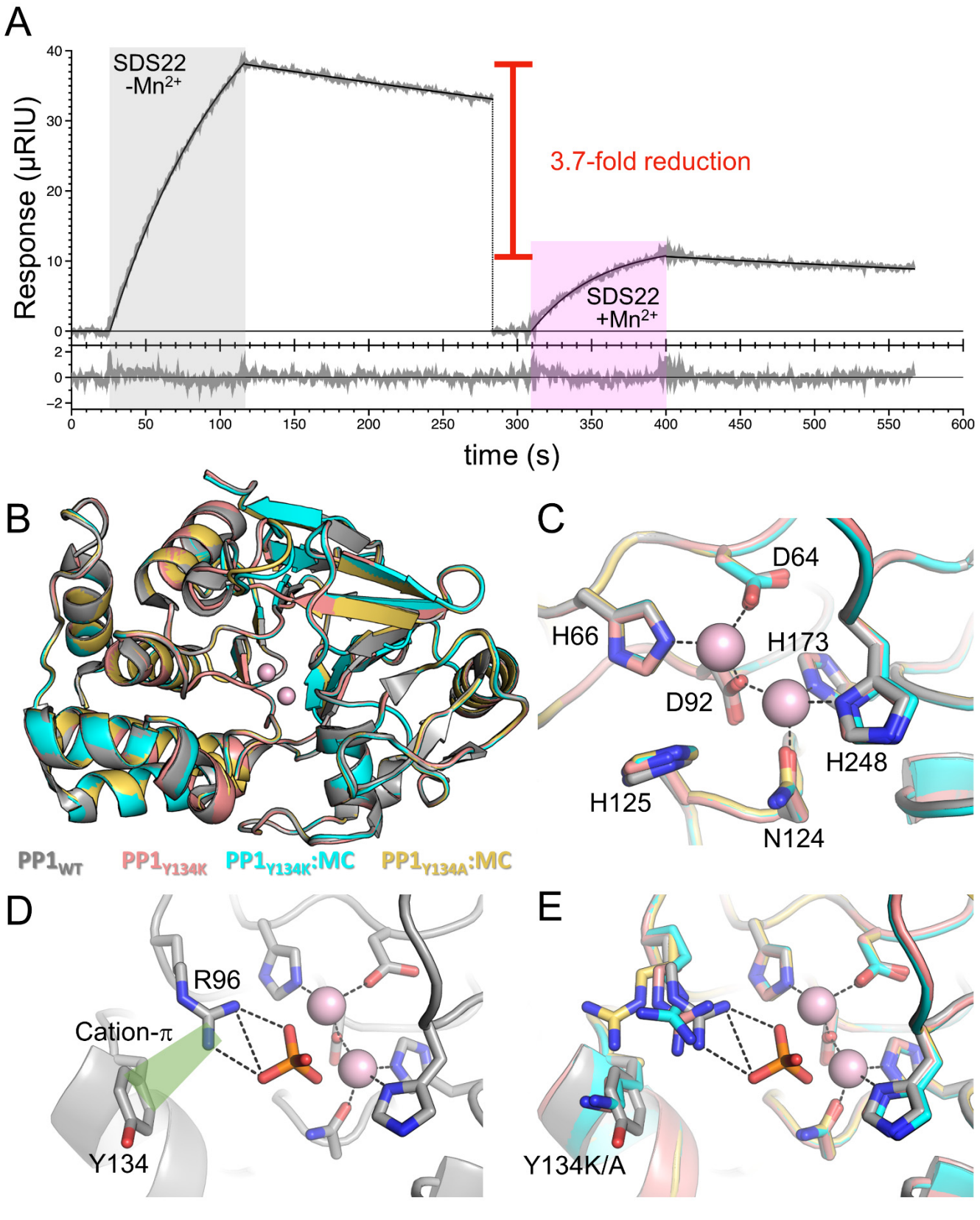
A
SDS22
-Mn2+
3.7-fold reduction
SDS22
+Mn2+
Response (μRIU)
time (s)
B
PP1WT
PP1Y134K
PP1Y134K:MC
PP1Y134A:MC
C
D64
H66
H173
D92
H248
H125
N124
D
R96
Cation-π
Y134
E
Y134K/A

Figure S8. ***Mn^{2+} competes with SDS22 for PP1 binding and the structures of PP1 variants Y134K and Y134A***. **A**. A representative sensorgram depicting 500 nM SDS22 binding to $PP1\alpha_{7-300}$ in the absence (grey, shaded area) or presence of $MnCl_2$ (0.25 mM, pink shaded area). There is a nearly 4-fold reduction in response of PP1 when SDS22 is injected in the presence of manganese, indicating that manganese can rapidly bind, change the conformation of PP1 and compete with SDS22 binding. **B**. Overlay of free PP1 (PDBID 4MOV; grey), $PP1_{Y134K}$ (salmon), $PP1_{Y134K}$:MC (cyan), $PP1_{Y134A}$:MC (gold) shows that there are no significant structural changes between wt PP1 and the Y134 variants. **C**. The active sites of $PP1_{Y134K}$, $PP1_{Y134K}$:MC and $PP1_{Y134A}$:MC adopt the metal-loaded conformation, with 2 metal ions (Mn^{2+}; pink spheres) at the active site just like $PP1_{WT}$ (grey). **D**. Residue Y134 orders R96 by forming a cation-π interaction. R96 is crucial for substrate (phosphate) recruitment at the active site. **E**. Y134K/A disrupts the cation-π interaction between Y134 and R96.

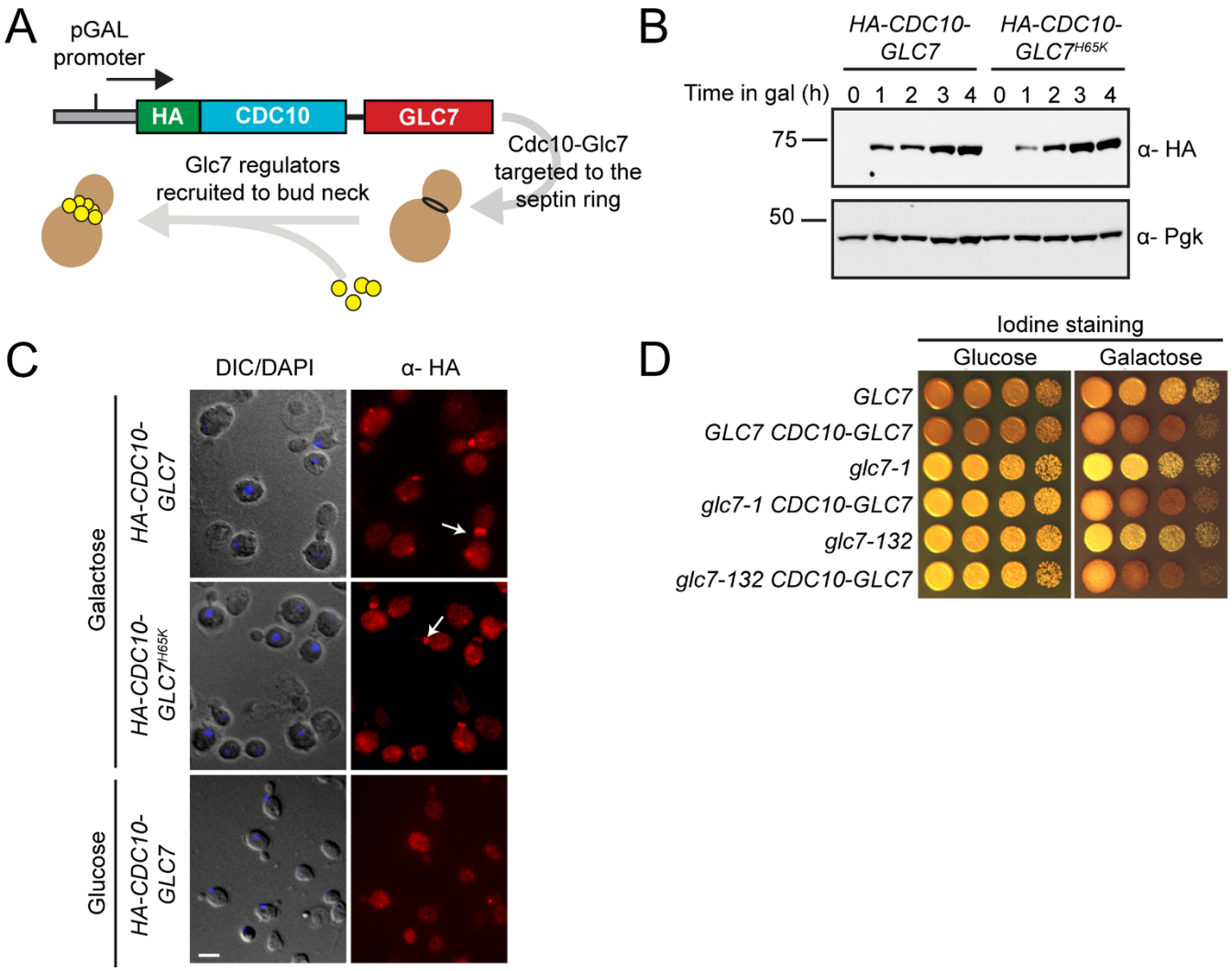

Figure S9. ***A platform for monitoring protein binding to nascent PP1***. Cdc10-Glc7 fusion is functional and targets to the bud neck. **A**. Model of the system: HA-CDC10-GLC7 chimera was placed under the transcriptional control of the *GAL1* promoter. A flexible linker was introduced between the 3' end of Cdc10 and the 5' end of Glc7 coding sequences to allow both proteins of the fusion to adopt native conformations. Upon induction, YFP-tagged Glc7 regulators (yellow spheres) are visualized at the bud neck. **B**. Immunoblot analysis of whole cell extracts from *CDC10-GLC7* (KT2954), *CDC10-GLC7*$_{H65K}$ (KT2986) strains grown to mid-log phase at 24°C, followed by induction with 2% galactose for the indicated times. Immunoblots were probed with anti-HA antibody to determine Cdc10-Glc7 protein levels and Pgk1 was used as the loading control. As can be seen, Cdc10-Glc7 is induced within one hour following the addition of galactose. **C**. Indirect immunofluorescence of HA-tagged Cdc10-Glc7 using anti-HA primary antibody and Alexa 546 secondary antibody. Cultures of *CDC10-GLC7* (KT4022 X KT4023) and *CDC10-GLC7*$_{H65K}$ (KT4020 X KT4021) strains were grown to mid-log phase at 24°C followed by induction with 2% galactose for 2 hours prior to preparation for indirect immunofluorescence, as described in material and methods. White arrows indicate Cdc10-Glc7 localization at the bud neck. Scale bar, 5 μm. **D**. To determine if the Cdc10-Glc7 fusion is functional, we assayed the

ability of the fusion to complement the glycogen deficiency of a glc7-1 mutant. glc7-1 mutants fail to accumulate glycogen (17), in part because the Glc7-1 protein cannot bind the glycogen targeting subunits (15) and hence, cannot activate glycogen synthase (18). Complementation of *glc7* mutations by *CDC10-GLC7* show that strains carrying *glc7-1* or another glycogen-deficient mutation, *glc7-132* (19), accumulate glycogen at levels comparable to the *WT* when expressing the *CDC10-GLC7* fusion gene. Cultures of the designated genotypes were serially diluted onto media containing glucose or galactose and incubated for 24h at 24°. Prior to image acquisition, the cells were exposed to iodine vapors to stain for glycogen (dark brown).

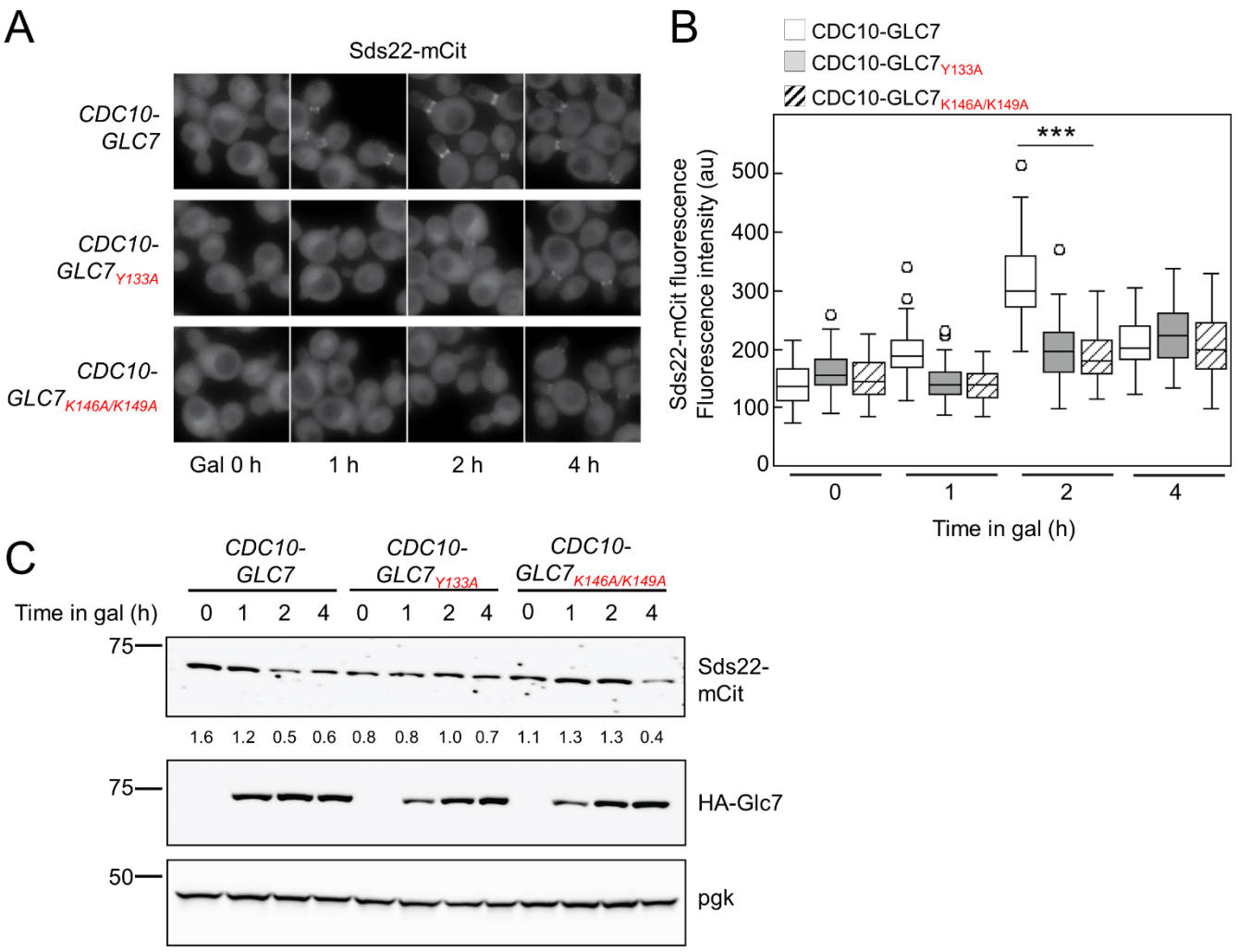

Figure S10. ***Low levels of Sds22 are recruited to the bud neck in cells expressing the Y133A and K146A/K149A Glc7 variants***. **A**. Sds22-mCit was imaged in CDC10-GLC7 (KT2926), CDC10-GLC7Y133A (KT4097) and CDC10-GLC7K146A K149A (KT4110) cells grown in galactose for the indicated times. **B**. Quantitative analysis of Sds22-mCit fluorescence in cells imaged in panel A. P values were calculated by two-tailed t-test (***=p<0.001). **C**. Immunoblot analysis of whole cell extracts from strains used in (A). with anti-GFP, anti HA and anti Pgk1 antibodies. Relative levels of Sds22-mCit quantified using Pgk1 as the loading control are shown below the Sds22 blot.

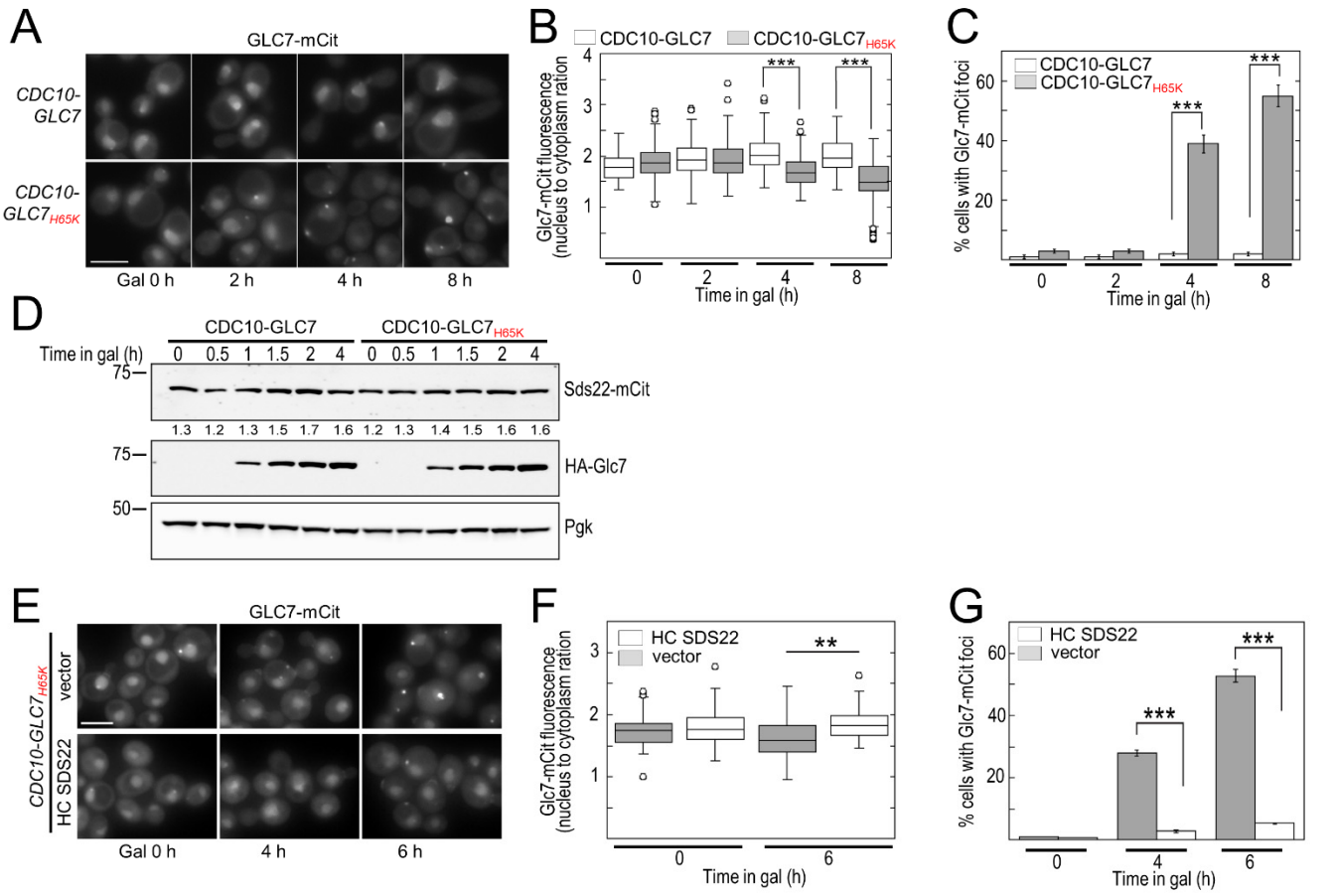

Figure S11. ***Mutations altering the GLC7 active site disrupt normal localization due to SDS22 sequestration – related to Figure 5***. **A.** Because our strains have a wild-type *GLC7* allele at its normal chromosomal position, we tested whether Cdc10 fused to the Glc7$_{H65K}$ variant interferes with WT Glc7 function. A Glc7-mCit strain (JRL852) transformed with plasmids containing either *CDC10-GLC7* or *CDC10-GLC7$_{H65K}$* was used to monitor the localization of endogenous Glc7-mCitrine (mCit) following Cdc10-Glc7/Cdc10-Glc7$_{H65K}$ induction. Transformants were grown in galactose for the indicated times and Glc7-mCit was imaged. Scale bar, 5μm. Strains expressing Cdc10-Glc7 (top panels) maintain normal nuclear localization of Glc7-mCit even after 8 hours in galactose. However, within 4 hours of inducing Cdc10-Glc7$_{H65K}$ (bottom panels), the nuclear/cytoplasmic ratio of Glc7-mCit is reduced with 55% of the cells showing bright Glc7 foci after 8 hours of Cdc10-Glc7$_{H65K}$ induction. These defects are reminiscent of the reduced nuclear Glc7 and bright puncta of aggregated Glc7 resulting from loss of function of several Glc7 regulators, including Sds22 and Ypi1 (Inhibitor-3) (20–24) showing Glc7$_{H65K}$ behaves as a dominant-negative mutant by interfering with normal Glc7 function. **B.** Nuclear to cytoplasmic ratio of Glc7-mCit fluorescence was quantified for cells described for (A) (n=100). **C**. Quantitative analysis of percentage cells from (A) possessing Glc7 foci. Error bars represent SD for three replicates (n=100 each). *P* values for (B) and (C) were calculated by two-tailed *t*-test (***=p<0.001). **D**. Immunoblot analysis of whole cell extracts from strains used in Figure 5C with anti-GFP, anti HA and anti Pgk1 antibodies. Relative levels of Sds22-mCit quantified using Pgk1 as the loading control are shown below the Sds22 blot. **E**. A Glc7-mCit strain (KT2492) was co-transformed with *CDC10-GLC7$_{H65K}$* and either the empty

vector (top panel) or HC SDS22 (bottom panel). The transformants were grown to mid-log phase in selective media for both plasmids and Glc7-mCit was imaged after addition of galactose for the indicated duration. Scale bar, 5µm. As can be seen, high copy *SDS22* also suppresses Glc7 dysregulation caused by Cdc10-Glc7$_{H65K}$ expression, as evident in higher nuclear-to-cytoplasmic ratios (compared to empty vector; see (F) and reduced formation of Glc7 foci (compared to empty vector; see (G)). These data show that the dominant negative effects of Cdc10-Glc7$_{H65K}$ on Glc7 localization and cell growth and division result from sequestration of Sds22, leading to inadequate availability of Sds22 for endogenous Glc7. **F**. Nuclear to cytoplasmic ratio of Glc7-mCit fluorescence was quantified for cells imaged in panel (E) (n=100). **G**. Quantitative analysis of percentage cells possessing Glc7 foci imaged in panel (E). Error bars represent SD for three replicates (n=100 each). *P* values for (F) and (G) were calculated by two-tailed *t*-test (***=p<0.001, **=p<0.005).

SUPPLEMENTAL REFERENCES

1. Choy MS, et al. (2014) Understanding the antagonism of retinoblastoma protein dephosphorylation by PNUTS provides insights into the PP1 regulatory code. *Proc Natl Acad Sci USA* 111(11):4097–4102.
2. Choy MS, Bolik-Coulon N, Archuleta TL, Peti W, Page R (2018) The structure of SDS22 provides insights into the mechanism of heterodimer formation with PP1. *Acta Crystallogr F Struct Biol Commun* 74(Pt 12):817–824.
3. O'Connell N, et al. (2012) The molecular basis for substrate specificity of the nuclear NIPP1:PP1 holoenzyme. *Structure* 20(10):1746–1756.
4. Heroes E, et al. (2019) Structure-Guided Exploration of SDS22 Interactions with Protein Phosphatase PP1 and the Splicing Factor BCLAF1. *Structure* 27(3):507-518.e5.
5. Emsley P, Lohkamp B, Scott WG, Cowtan K (2010) Features and development of Coot. *Acta Crystallogr D Biol Crystallogr* 66(Pt 4):486–501.
6. Adams PD, et al. (2010) PHENIX: a comprehensive Python-based system for macromolecular structure solution. *Acta Crystallogr D Biol Crystallogr* 66(Pt 2):213–221.
7. Karlsson R, Katsamba PS, Nordin H, Pol E, Myszka DG (2006) Analyzing a kinetic titration series using affinity biosensors. *Anal Biochem* 349(1):136–147.
8. Sherman F, Fink, GR, Hicks JB (1986) *Methods in Yeast Genetics* (Cold Spring Harbor Laboratory Press, Cold Spring Harbor, NY).
9. Rose MDF, Winston F, Hieter, P. (1990) *Methods in Yeast Genetics. A Laboratory Course Manual* (Cold spring Harbor Laboratory Press, Cold Spring Harbor, NY).
10. Chester VE (1968) Heritable glycogen-storage deficiency in yeast and its induction by ultra-violet light. *J Gen Microbiol* 51(1):49–56.
11. Larson JR, et al. (2008) Protein phosphatase type 1 directs chitin synthesis at the bud neck in Saccharomyces cerevisiae. *Mol Biol Cell* 19(7):3040–3051.
12. Foreman PK, Davis RW (1994) Cloning vectors for the synthesis of epitope-tagged, truncated and chimeric proteins in Saccharomyces cerevisiae. *Gene* 144(1):63–68.
13. Berkower C, Loayza D, Michaelis S (1994) Metabolic instability and constitutive endocytosis of STE6, the a-factor transporter of Saccharomyces cerevisiae. *Mol Biol Cell* 5(11):1185–1198.
14. Ravindran R, Polk P, Robinson LC, Tatchell K (2018) New ubiquitin-dependent mechanisms regulating the Aurora B-protein phosphatase 1 balance in Saccharomyces cerevisiae. *J Cell Sci* 131(16). doi:10.1242/jcs.217620.
15. Stuart JS, Frederick DL, Varner CM, Tatchell K (1994) The mutant type 1 protein phosphatase encoded by glc7-1 from Saccharomyces cerevisiae fails to interact productively with the GAC1-encoded regulatory subunit. *Mol Cell Biol* 14(2):896–905.
16. Frederick DL, Tatchell K (1996) The REG2 gene of Saccharomyces cerevisiae encodes a type 1 protein phosphatase-binding protein that functions with Reg1p and the Snf1 protein kinase to regulate growth. *Mol Cell Biol* 16(6):2922–2931.
17. Cannon JF, Pringle JR, Fiechter A, Khalil M (1994) Characterization of glycogen-deficient glc mutants of Saccharomyces cerevisiae. *Genetics* 136(2):485–503.
18. Anderson C, Tatchell K (2001) Hyperactive glycogen synthase mutants of Saccharomyces cerevisiae suppress the glc7-1 protein phosphatase mutant. *J Bacteriol* 183(3):821–829.
19. Baker SH, Frederick DL, Bloecher A, Tatchell K (1997) Alanine-scanning mutagenesis of protein phosphatase type 1 in the yeast Saccharomyces cerevisiae. *Genetics* 145(3):615–626.

20. Bharucha JP, Larson JR, Gao L, Daves LK, Tatchell K (2008) Ypi1, a positive regulator of nuclear protein phosphatase type 1 activity in Saccharomyces cerevisiae. *Mol Biol Cell* 19(3):1032–1045.
21. Cheng Y-L, Chen R-H (2015) Assembly and quality control of the protein phosphatase 1 holoenzyme involves the Cdc48-Shp1 chaperone. *J Cell Sci* 128(6):1180–1192.
22. Pedelini L, et al. (2007) YPI1 and SDS22 proteins regulate the nuclear localization and function of yeast type 1 phosphatase Glc7. *J Biol Chem* 282(5):3282–3292.
23. Peggie MW, et al. (2002) Essential functions of Sds22p in chromosome stability and nuclear localization of PP1. *J Cell Sci* 115(Pt 1):195–206.
24. Robinson LC, Phillips J, Brou L, Boswell EP, Tatchell K (2012) Suppressors of ipl1-2 in components of a Glc7 phosphatase complex, Cdc48 AAA ATPase, TORC1, and the kinetochore. *G3 (Bethesda)* 2(12):1687–1701.